The origin of the atomic and molecular gas contents of early-type galaxies – II. Misaligned gas accretion

Claudia del P. Lagos,[1][*] Nelson D. Padilla,[2,3] Timothy A. Davis,[1,4] Cedric G. Lacey,[5] Carlton M. Baugh,[5] Violeta Gonzalez-Perez,[5] Martin A. Zwaan[1] and Sergio Contreras[2]

[1]*European Southern Observatory, Karl-Schwarzschild-Strasse 2, D-85748, Garching, Germany*
[2]*Instituto de Astrofísica, Pontificia Universidad Católica de Chile, Av. Vicuña Mackenna 4860, Santiago, Chile*
[3]*Centro de Astro-Ingeniería, Pontificia Universidad Católica de Chile, Av. Vicuña Mackenna 4860, Santiago, Chile*
[4]*Centre for Astrophysics Research, Science & Technology Research Institute, University of Hertfordshire, Hatfield AL10 9AB, UK*
[5]*Institute for Computational Cosmology, Department of Physics, University of Durham, South Road, Durham DH1 3LE, UK*

ABSTRACT

We study the origin of the wide distribution of angles between the angular momenta of the stellar and gas components, $\alpha_{G,S}$, in early-type galaxies (ETGs). We use the GALFORM model of galaxy formation, set in the Λ cold dark matter framework, and coupled it with a Monte Carlo simulation to follow the angular momenta flips driven by matter accretion on to haloes and galaxies. We consider a gas disc to be misaligned with respect to the stellar body if $\alpha_{G,S} > 30$ deg. By assuming that the only sources of misalignments in galaxies are galaxy mergers, we place a lower limit of 2–5 per cent on the fraction of ETGs with misaligned gas/stellar components. These low fractions are inconsistent with the observed value of $\approx 42 \pm 6$ per cent in ATLAS^{3D}. In the more general case, in which smooth gas accretion in addition to galaxy mergers can drive misalignments, our calculation predicts that ≈ 46 per cent of ETGs have $\alpha_{G,S} > 30$ deg. In this calculation, we find correlations between $\alpha_{G,S}$ and stellar mass, cold gas fraction and star formation rate, such that ETGs with high masses, low cold gas fractions and low star formation rates are more likely to display aligned cold gas and stellar components. We confirm these trends observationally for the first time using ATLAS^{3D} data. We argue that the high fraction of misaligned gas discs observed in ETGs is mostly due to smooth gas accretion (e.g. cooling from the hot halo of galaxies) which takes place after most of the stellar mass of the galaxy is in place and comes misaligned with respect to the stellar component. Galaxies that have accreted most of their cold gas content prior to the time where most of the stellar mass was in place show aligned components.

Key words: galaxies: elliptical and lenticular, cD – galaxies: evolution – galaxies: formation – galaxies: ISM – galaxies: kinematics and dynamics.

1 INTRODUCTION

Contrary to naive expectations, early-type galaxies (ETGs, ellipticals and lenticulars), host significant quantities of cold gas in the form of atomic hydrogen (H I) and molecular hydrogen (H$_2$), although the gas fractions in ETGs are on average lower than in late-type galaxies (LTGs; e.g. Gallagher, Faber & Balick 1975; Wardle & Knapp 1986; Wiklind & Henkel 1989; Morganti et al. 2006; Oosterloo, Fraternali & Sancisi 2007; Welch, Sage & Young 2010; Young et al. 2011; Serra et al. 2012). Serra et al. (2012) found that 42 per cent of ETGs in the ATLAS^{3D} have H I masses

$M_{H_I} > 10^7 \, M_\odot$, while Young et al. (2011) show that 23 per cent of ETGs have $M_{H_2} > 10^7 \, M_\odot$ in the same survey. Most ETGs with detected H I and/or H$_2$ show settled configurations, with the cold gas being in a disc or a ring (Serra et al. 2012; Davis et al. 2013). Only 30 per cent of ETGs with detected H I show unsettled configurations. This has been interpreted as being due to interactions with the group environments or a recent minor galaxy merger (Serra et al. 2012). This percentage decreases when focusing on H$_2$ only (Alatalo et al. 2013; Davis et al. 2013).

Lagos et al. (2014b, hereafter Paper I) explored the origin of the H I and H$_2$ gas contents of ETGs using a semi-analytic model of galaxy formation and showed that the observed gas fractions in ETGs arise in the model due to inefficient replenishment of the gas in ETGs as a result of both ram-pressure stripping of the

[*] E-mail: clagos@eso.org

hot gas and heating by active galactic nuclei (AGN), which prevents gas cooling from the hot halo. Model ETGs with high H I and H₂ gas contents were shown to be hosted by low-mass haloes, and have, on average, 'younger morphologies' (i.e. smaller look-back times to the last time these ETGs showed late-type morphologies). These ETGs were shown in Paper I to be more isolated, which agrees with observational inferences of lower density environments for the gas-rich ETGs (Young et al. 2014).

An important finding in the exhaustive observations of the kinematics of the different mass components of ETGs was presented in Davis et al. (2011), where it was convincingly shown that ≈42 per cent of ETGs have ionized gas misaligned with the stellar kinematics (i.e. the angle between the angular momenta of the stars and the gas is >30 deg). The way the angle between the different galaxy components is measured in the observations is using high signal-to-noise ratio (S/N > 40; Emsellem et al. 2004) integral field spectroscopy and millimetre wave interferometry, from which one can construct 2D kinematic maps. Davis et al. (2011) calculated position angles from the 2D kinematic maps of the stellar and gas components in a way that they trace the bulk of the components rather than substructures. From the position angles, the projected misalignments, rather than the 3D misalignments, were measured. Typical uncertainties in the measured position angles in ATLAS³ᴰ are of 10 deg. Davis et al. (2011) also show that the molecular and ionized gas components are aligned with each other, suggesting a common origin.

The high fraction of stellar/gas misalignments reported by Davis et al. (2011) led to speculation that the origin of this gas is external, pointing to minor mergers as the dominant source of the gas in ETGs that show misaligned gas discs (e.g. Davis et al. 2011; Serra et al. 2012). This intriguing inference has been explored in simulations of galaxy formation very recently, with small samples of simulated galaxies. For example, Serra et al. (2014) show that although simulations can reproduce the nature of slow and fast rotators of the early-type population (see also Naab et al. 2014), the H I contents predicted by these simulations are too low, while also being almost always kinematically aligned with the stellar component. The main disadvantage of the work of Serra et al. is that only 50 simulated galaxies were analysed and therefore strong conclusions regarding the consistency of the simulations with observations cannot be reached.

An important caveat in the interpretation presented by Davis et al. (2011) and Serra et al. (2012), in which only minor galaxy mergers account for the misaligned gas discs observed in ETGs, is that it ignores the stochastic nature of matter accretion from sources (other than mergers) predicted in a Λ cold dark matter (ΛCDM) universe (e.g. Dekel, Sari & Ceverino 2009; Johansson, Naab & Ostriker 2012). It implies that gas accretion from sources other than galaxy mergers, such as cooling from the hot halo and collimated inflows of gas from filaments, is always aligned with the stellar component. Sales et al. (2012), Sharma, Steinmetz & Bland-Hawthorn (2012), Bett & Frenk (2012), Aumer et al. (2013) and Padilla et al. (2014) show strong evidence from simulations that in a ΛCDM universe the angular momentum of galaxies is not necessarily aligned with that of their host haloes, as accretion from either the cosmic web or mergers can be stochastic. Bett & Frenk (2012) go a step further and show that the inner parts of haloes, where galaxies live, can suffer much more frequent flips of their angular momentum vector than the halo as a whole (see also Sharma et al. 2012).

Bett et al. (2010) show that the median angle between the inner ($\lesssim 0.25\,R_{vir}$) and total ($\leq R_{vir}$) angular momentum vectors is

≈25 deg. Bett et al. also show that the inclusion of baryons drives even larger misalignments, with half of the galaxies having their spin axis misaligned by more than 45 deg from the host halo spin (see also Bryan et al. 2013; Tenneti et al. 2014). There is also evidence from hydrodynamical simulations that the angular momentum of galaxies is affected by the large-scale structure; i.e. filamentary structure can fuel gas into galaxies changing its angular momentum direction (e.g. Danovich et al. 2014; Dubois et al. 2014). The result of such accretion process can be alignment with respect to large structures, outside haloes, particularly in the low-mass regime (Dubois et al. 2014).

Our motivation is therefore to investigate the alignments between the galaxy components, stars and cold gas (atomic and molecular gas), and the dark matter (DM) halo by following the flips in the angular momentum of ETGs throughout their growth history. By flips we mean any change in the direction of the angular momentum vector. This allows us to statistically assess the probability of having a present-day ETG with a gas disc that is misaligned with respect to the stellar component. For consistency with the measured projected misalignment angle between different galaxy components in the observations, we show throughout the paper predictions of projected misalignments. The study of angular momentum in galaxies is particularly relevant as ongoing and future surveys, such as Mapping Nearby Galaxies at APO (MaNGA)[1], Calar Alto Legacy Integral Field spectroscopy Area survey (CALIFA[2]), the Sydney-Australian-Astronomical-Observatory Multi-object Integral-Field Spectrograph (SAMI)[3] and ultimately the Square Kilometre Array (SKA)[4], promise to transform our understanding of angular momentum in galaxies in their different components. An example of this is the mass–spin–morphology relation presented by Obreschkow & Glazebrook (2014).

For this study, we use the semi-analytical model GALFORM in a ΛCDM cosmology (Cole et al. 2000) presented by Lacey et al. (in preparation). This model includes the improved treatment of star formation (SF) implemented by Lagos et al. (2011a,b). This extension explicitly splits the hydrogen content of the ISM of galaxies into H I and H₂. In Paper I, we show that the Lacey et al. model provides a very good representation of the gas contents of ETGs (in the form of H I and H₂) in the local Universe, particularly when gradual ram-pressure stripping of the hot gas is included (see Lagos et al. 2014a for predictions of the gas content of galaxies in the Lacey et al. model at high redshifts).

This paper is organized as follows. In Section 2, we summarize the main aspects of the GALFORM model and the flavour presented by Lacey et al. (in preparation). In Section 3, we summarize the method for following the flips in the angular momenta of the different component of galaxies (stars, cold gas and DM halo), originally introduced by Padilla et al. (2014). In Section 4, we present the growth history of ETGs and analyse the transient nature of galaxy morphologies. In Section 5, we describe how we calculate the angular momentum flips throughout the history of ETGs and present the expectation for the number of misaligned gas discs and compare with observations. We also introduce a new scenario that can lead to gas discs becoming misaligned in addition to galaxy mergers. In Section 6, we discuss limitations of the model presented here,

---

[1] https://www.sdss3.org/future/manga.php

[2] http://califa.caha.es/ (Husemann et al. 2013).

[3] http://sami-survey.org/ (Croom et al. 2012).

[4] https://www.skatelescope.org/

also showing predictions for LTGs, and give our conclusions in Section 7.

2 MODELLING THE MORPHOLOGICAL EVOLUTION, NEUTRAL GAS CONTENT AND SF IN GALAXIES

In Paper I, we provided a detailed description of all the relevant physical mechanisms which affect the history of ETGs, such as disc formation, bulge formation, ram-pressure stripping of the hot gas, SF and recycling of mass and metals in stars. Here, we outline the processes that are modelled in GALFORM and give a brief overview of the model we adopt as a standard in this paper to study the alignment between cold gas and stars in galaxies, which is a variant of the model of Lacey et al. (in preparation).

GALFORM accounts for the main physical processes that shape the formation and evolution of galaxies. These are: (i) the collapse and merging of DM haloes, (ii) the shock heating and radiative cooling of gas inside DM haloes, leading to the formation of galactic discs, (iii) SF in galaxy discs (quiescent mode), (iv) feedback from supernovae (SNe), from heating by AGN and from photoionization of the intergalactic medium, (v) chemical enrichment of stars and gas, (vi) galaxy mergers driven by dynamical friction within common DM haloes which can trigger bursts of SF, and lead to the formation of spheroids, (vii) global disc instabilities, which also lead to the formation of spheroids and (viii) gradual ram-pressure stripping of the hot gas. Galaxy luminosities are computed from the predicted SF and chemical enrichment histories using a stellar population synthesis model (see Gonzalez-Perez et al. 2014). Note that in the literature 'quiescent' is generally used to refer to passive galaxies and/or to those with low star formation rates (SFRs) compared to the median at a given stellar mass, but here we use it to distinguish SF taking place in the disc of galaxies from the starburst mode, which takes place exclusively in the central spheroid of the galaxy and at efficiencies that are generally higher.

Here, we focus on the variant of GALFORM presented in Lacey et al. (in preparation, hereafter Lacey14) which includes all the processes listed above. One important feature of the Lacey14 model is that it adopts a non-universal stellar initial mass function (IMF). The IMF describing SF in discs (i.e. the quiescent mode) is the Kennicutt (1983) IMF,[5] while a more top-heavy IMF is adopted in starbursts (i.e. with an IMF slope $x = 1$). This is inspired by Baugh et al. (2005), who used a top-heavy IMF to reconcile the model predictions with observations of the number counts and redshift distribution of submillimetre galaxies. We note, however, that Baugh et al. adopted a more top-heavy IMF for starbursts, with $x = 0$, than is used for Lacey14.

We now give some details of each of the processes above as included in Lacey14.

(i) In Lacey14, the halo merger trees are extracted from the *WMAP*7 (Komatsu et al. 2011) version of the Millennium cosmological *N*-body simulation (Springel et al. 2005, refer to as MS-W7 simulation). The cosmological parameters are $\Omega_m = \Omega_{DM} + \Omega_{baryons} = 0.272$ (with a baryon fraction of 0.167), $\Omega_\Lambda = 0.728$, $\sigma_8 = 0.81$ and $h = 0.704$.

---

[5] The distribution of the masses of stars produced follows $dN(m)/d\ln m \propto m^{-x}$, where N is the number of stars of mass m formed, and x is the IMF slope. For a Kennicutt (1983) IMF, $x = 1.5$ for masses in the range $1\,M_\odot \leq m \leq 100\,M_\odot$ and $x = 0.4$ for $m < 1\,M_\odot$.

(ii) Gas cooling is calculated assuming that gas in haloes follows a β profile (Cavaliere & Fusco-Femiano 1976). The amount of cooling then depends on the gas density and its metallicity following the tabulated cooling function of Sutherland & Dopita (1993). The amount of gas that is added to the disc depends on the cooling time and the free-fall time (see Cole et al. 2000; Benson & Bower 2010). Given the time elapsed since the formation of the DM halo (i.e. the last mass doubling), the free-fall radius, r_{ff}, is the maximum radius in the hot halo from which material could have moved to the disc; the cooling radius, r_{cool}, encloses the radius within which gas has had time to cool. The mass accreted on to the disc simply corresponds to the hot gas mass enclosed within $r = \min[r_{cool}, r_{ff}]$.

(iii) Lacey14 adopts two different SF laws, one for quiescent SF (i.e. taking place in the disc) and another for starbursts (driven by galaxy mergers and disc instabilities). In the case of quiescent SF, Lacey14 adopts the SF law introduced by Blitz & Rosolowsky (2006), where stars form from the molecular gas in the disc, and the partition of atomic and molecular gas depends on the hydrostatic pressure in the mid-plane of the disc (see Lagos et al. 2011a for details). For starbursts, the SFR is calculated from the available cold gas mass (H I plus H_2), regulated by a SF time-scale, τ_{SF}, which depends on the dynamical time-scale of the bulge, τ_{dyn}, $\tau_{SF} = \max(\tau_{min}, f_{dyn}\tau_{dyn})$. The proportionality $f_{dyn} = 20$ is a free parameter, and τ_{min} is a minimum starburst duration, which is set to $\tau_{min} = 100\,Myr$.

(iv) The mass entrainment of SNe driven winds, β, in GALFORM is parametrized by the circular velocity of the galaxy, taken to be a proxy for the gravitational potential well. In Lacey14, $\beta = (V_{circ}/320\,km\,s^{-1})^{-3.2}$. Detailed calculations of SNe feedback suggest the power-law index of this parametrization should be in the range -1 to -2.7 (Murray, Quataert & Thompson 2005; Creasey, Theuns & Bower 2013; Lagos, Lacey & Baugh 2013). The power-law index of -3.2 in Lacey14 comes from the Monte Carlo exploration of parameters originally done in Bower et al. (2006), which pointed to that value as the best parameter to recover a flat faint-end in the *K*-band luminosity function. However, since this value is in tension with the more recent studies above, we are currently exploring the effect of including more physical parametrizations (Mitchell et al. 2014; Mitchell et al., in preparation). However, we expect the effect of these new parametrizations on the conclusions presented in this paper to be secondary. This is because the selected model ETGs for the study here are relatively massive $L_K > 6 \times 10^9\,M_\odot$, and more affected by AGN feedback (see Paper I for details).

(v) In GALFORM AGN feedback is assumed to act in haloes where the cooling time is longer than the free-fall time at the cooling radius ('hot accretion' mode; Fanidakis et al. 2012). In such a halo, the AGN power is computed and if it is greater than the cooling luminosity, the cooling flow is switched off (see Bower et al. 2006).

(vi) For photoionization feedback, it is assumed that no gas is allowed to cool in haloes with a circular velocity below V_{crit} at redshifts below z_{reion} (Benson et al. 2002). Taking into account simulations by Okamoto, Gao & Theuns (2008) and observational constraints on the reionization redshift (Komatsu et al. 2011), Lacey14 adopt $V_{crit} = 30\,km\,s^{-1}$ and $z_{reion} = 10$.

(vii) For chemical enrichment, we adopt the instantaneous mixing approximation for metals in the ISM, and change the amount of metals recycled depending on the IMF adopted. The stellar evolution models of Marigo (2001) and Portinari, Chiosi & Bressan (1998) are adopted to calculate the ejected mass and metals from intermediate and massive stars, respectively.

(viii) Lacey14 adopt the updated dynamical friction time-scale of Jiang et al. (2008) to estimate the time-scale for the orbital decay

of satellite galaxies towards the centre. This decay is due to energy and angular momentum losses driven by dynamical friction with the DM halo material. Once the galaxy merger takes place, a starburst takes place in the centre, where the SFR is taken to be proportional to the amount of cold gas (H I plus H$_2$) in the system, regulated by a SF time-scale. This SF time-scale is calculated as described above. Note that the Jiang et al. (2008) formula is an update of the widely used Lacey & Cole (1993) dynamical friction time-scale, using recent *N*-body simulations.

(ix) Global disc instabilities in galaxies occur if the disc becomes sufficiently massive that its self-gravity is dominant over the pressure produced by rotation. In this case, the disc becomes unstable to small perturbations caused by minor satellites or DM substructures. The criterion for instability was described by Efstathiou, Lake & Negroponte (1982), Mo, Mao & White (1998) and Cole et al. (2000). SF in the case of instabilities proceeds as in starbursts driven by galaxy mergers. It is important to remark here that the way disc instabilities are treated in GALFORM are a simplification of what detailed simulations show. For example, Ceverino, Dekel & Bournaud (2010) and Bournaud et al. (2011, 2014) show that when discs are globally unstable, large clumps of gas are formed that can be long lived due to the large accretion rates that counteract the mass-loss due to outflows and stripping. These long-lived clumps can migrate to the central parts of the galaxy and build a large bulge in less than 1 Gyr. This is captured in our simplified model through the triggering of a starburst in the central bulge of galaxies. However, contrary to our assumption here, simulations show that the disc is not fully destroyed in the process of disc instability. We plan to investigate the effect this has on the history of ETGs in a future paper.

(x) The standard treatment of the hot gas in the subhaloes around satellite galaxies is usually referred to as 'strangulation' of the hot gas, which means that once a galaxy becomes a satellite (when it crosses the virial radius of the larger halo), its hot gas is removed instantaneously and is transferred to the hot gas reservoir of the main halo. This is the model adopted in the default Lacey14 model. However, in Paper I we show that this treatment is too extreme and leads to ETGs having too low H I and H$_2$ gas fractions compared to observations. In Paper I, we argue that gradual ram-pressure stripping of the hot gas is needed in order to bring gas fractions into agreement with observations. The latter is calculated by considering the ram pressure of the hot gas in the main halo acting against the hot gas of the satellite galaxy as it moves through the halo, and the gravity of the satellite retaining part of the hot halo (see Font et al. 2008; McCarthy et al. 2008). The Lacey14 model including this scheme of gradual ram-pressure stripping of the hot gas is referred to as Lacey14+GRP (gradual ram pressure). The latter is our standard model for the rest of the paper, which we show in Paper I to provide H I and H$_2$ gas fractions and mass functions in very good agreement with the observations of the ATLAS^{3D} and HIPASSs (HI Parkes All Sky Surveys). Note that we do not include ram-pressure stripping of the cold gas disc of galaxies. Although this process has been shown to be important in cluster environments (e.g. Cortese et al. 2011; Boselli et al. 2014), most ETGs in the model and in ATLAS^{3D} reside in environments other than galaxy clusters, and therefore we do not expect this process to change the conclusions we present in this paper (see Paper I for more details).

(xi) To calculate the circular velocity and size of the galaxy disc in GALFORM, it is assumed that there is conservation of angular momentum and centrifugal equilibrium in the process of gas cooling, while for the size of bulges, energy conservation and virial equilibrium are assumed during galaxy mergers or disc instabilities. In addition, the mass distribution in the halo and the length-scales

of the disc and the bulge adjust adiabatically in response to their mutual gravity.

3 FOLLOWING FLIPS IN THE ANGULAR MOMENTUM OF THE GAS, STARS AND DM HALO

We use the Monte Carlo based method developed by Padilla et al. (2014) to follow the flips in the angular momenta of the cold gas (atomic plus molecular) and stars in galaxies, and the DM halo. Padilla et al. based their study on the Millennium-II simulation (Boylan-Kolchin et al. 2009), which has a resolution that is 125 times better than the Millennium simulation described in Section 2. This allowed Padilla et al. to accurately calculate the angular momentum, J, in all DM haloes and subhaloes with masses $\gtrsim 10^{10} \, h^{-1} \, M_{\odot}$, based on at least 1000 particles.[6] Thus, the direction of J can be accurately traced before and after accretion of matter and merger events. Padilla et al. built a probability distribution function (PDF) for the angle between J before and after the accretion, $\Delta\alpha_{DM}$, which depends on the relative change in mass. There are also variations with redshift, due to the expansion of the universe and the relative angular momentum brought by the material as time passes. Thus, we build the PDFs for different redshifts and relative mass changes. In addition, smooth accretion of matter (which is from the cosmic web and it is not resolved in individual haloes) and halo mergers drive different magnitudes of angular momentum flips even though they may cause a similar change in mass, with halo mergers tending to drive higher $\Delta\alpha_{DM}$ than accretion on to haloes (see Appendix A for the PDFs produced by Padilla et al.).

The strongest assumption Padilla et al. make to apply this methodology to galaxies is that accretion on to galaxies produces flips in the angular momenta, $\Delta\alpha_{bar}$, of the same order as in the haloes (namely, it will depend on the relative change in mass, on the nature of the accretion, i.e. whether it is from smooth accretion or mergers, and on time), $\Delta\alpha_{bar}(\Delta M_{bar}|M_{bar}, t) \equiv \Delta\alpha_{DM}(\Delta M_{DM}|M_{DM}, t)$. In other words, Padilla et al. sample the PDFs created from the Millennium-II simulation to find by how much the angular momentum of a galaxy flips due to accretion. This can be done for the different galaxy components.

Padilla et al. (2014) implemented the method above in the semi-analytic model SAG (Lagos, Cora & Padilla 2008; Jiménez et al. 2011), modifying the specific angular momentum of galaxies in the model. This also affects the sizes of galaxies and therefore SF and the strength of feedback. Padilla et al. did not change any model parameters and show the effect of this new physical model on galaxy properties. Ruiz et al. (2013) presented the recalibration of the Padilla et al. (2014) model and the fits to the stellar mass function.

Here, we apply the Padilla et al. (2014) model as post-processing to GALFORM to calculate the flips in the direction of the angular momentum of ETGs due to their growth history, but we do not modify the sizes of galaxies or any other property as a result. For this reason, there is no need for changing any parameter in the model. By post-processing GALFORM using the Padilla et al. Monte Carlo method, we can accumulate the flips of the angular momentum vector of the gas disc and, based on the assumption that new stars form perfectly aligned with the gas disc at the time they form,

---

[6] Note that in Millennium-I a halo of mass $10^{10} \, h^{-1} \, M_{\odot}$ is resolved with 10 particles only, which makes the measurements of angular momentum very noisy.

we can calculate the angle between the angular momenta of the gas disc and the stellar body at each timestep in the evolution of galaxies. Although these changes are expected in such a model, Padilla et al. (2014) show that the changes are not major except in the fraction of massive galaxies that are ETGs, in a way that the model including the change in the specific angular momentum due to flips in the direction of the angular momentum vector produces a higher fraction of ETGs than the previous model. We therefore do not expect a self-consistent calculation to strongly change the conclusions we present in this paper.

We can take the predicted history of each ETG in our simulation (based on the Lacey14+GRP model) and calculate the angle between the gas and stars in galaxies and the DM halo. The history of ETGs is fully characterized by minor and major merger events, disc instabilities, accretion of gas from the halo, outflow gas to the halo by recent SF (SNe feedback), mass-loss from intermediate- and low-mass stars to the ISM, and heating of the halo gas due to the energy injected there by the AGN (AGN feedback). All these events will change the gas and stellar contents of ETGs.

The way we apply the Padilla et al. methodology to our galaxies is as follows.

(i) In an individual halo, the angular momenta of the hot gas and DM are perfectly aligned before the first galaxy forms.

(ii) When the first galaxy forms, the gas cools down preserving the specific angular momentum of the hot gas and its direction, leading to a gas disc that is perfectly aligned with the hot halo (see panel i in Fig. 1). Since stars form from this gas disc, they will also be aligned with the gas and hot halo components.

(iii) When a DM halo of mass M_{DM} accretes matter, ΔM_{DM}, at a time t, it flips its angular momentum direction by an angle $\Delta \alpha_{DM}(\Delta M_{DM}|M_{DM}, t)$. This change is instantly propagated to the angular momentum of the hot gas (see panel ii in Fig. 1). As a result, there will be some level of misalignment between the gas in the disc that cooled from the hot gas before it flipped and the DM halo. Note that the instantaneous reaction of the hot halo assumed here is for simplicity. In reality, there is a torque time-scale associated with this process, although this should act on a relatively short time-scale of the order of the dynamical time-scale of the halo. The stars remain fully aligned with the cold gas disc.

(iv) When new gas cools down from the flipped hot gas halo, it comes misaligned with the existing gas and stellar disc (see panel ii in Fig. 1). The time-scale for this gas to cool down and be accreted on to the galaxy disc is calculated as described in Section 2 (second bullet point). The cooled gas will change the direction of the angular momentum vector of the cold gas disc towards that of the hot halo (see panel iii in Fig. 1). The resulting cold gas disc will form stars, and will also change the direction of the angular momentum vector of the stellar disc towards that of the cold gas disc (as in panel iv in Fig. 2). Depending on the cooled mass and the mass of the newly formed stars relative to the existing disc, there will be a remaining angle between the angular momenta of the cold gas and stellar discs (panel v in Fig. 2). The resulting flip in the angular momentum direction of the cold gas and stellar components are calculated as a mass-weighted angle. From this it is implicit that the stars will have an angular momentum direction set mainly by the angular momentum direction of stars at the time of the peak of the SF activity.

(v) When there is a process such as disc instabilities or galaxy mergers that drive the formation of galaxy bulges from a pre-existing stellar disc, we assume that the newly formed bulge preserves the direction of the angular momentum the stellar disc had. Any further
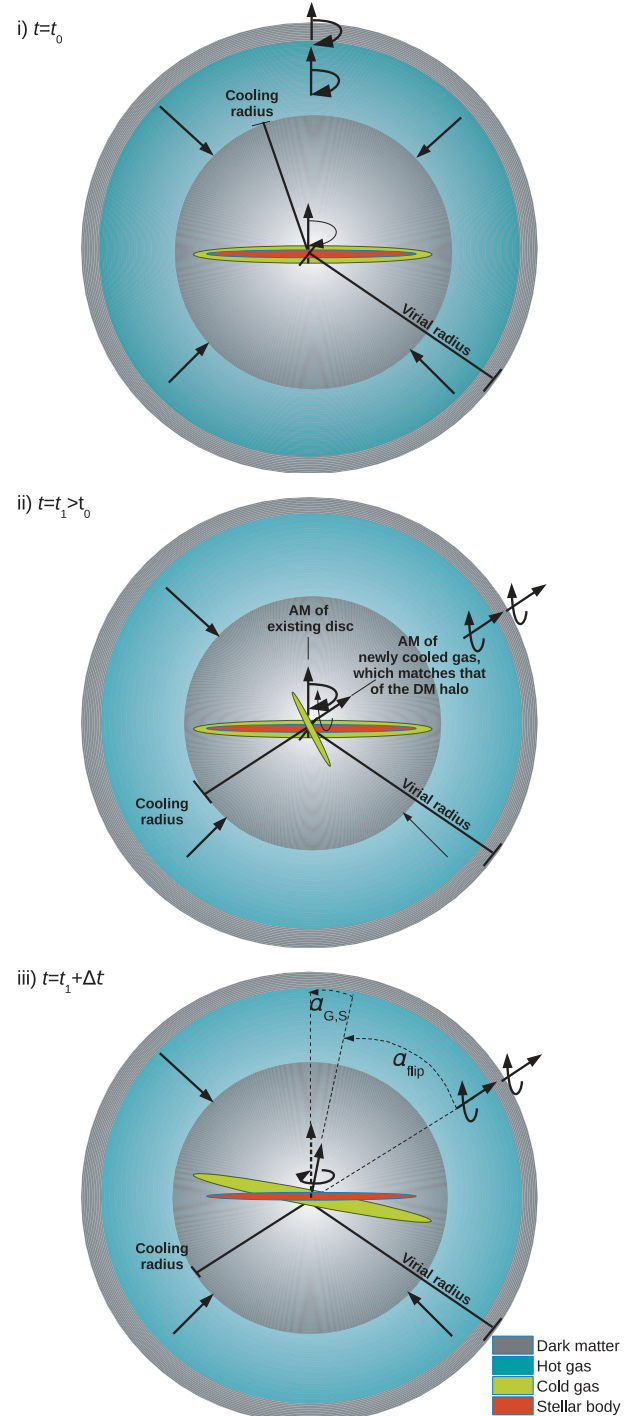
Figure 1. Schematic showing the methodology of Padilla et al. (2014) applied to our simulated ETGs. In panel (i) we show a recently formed galaxy, in which all the components have angular momenta that are perfectly aligned. In a later timestep, t_1 (panel ii), the DM halo and hot gas flip their angular momenta direction due to accretion. This flip can only be propagated to the galaxy by the accretion of cooled gas from the hot halo, which is shown as a condensation of cold gas with a spin aligned with the DM halo. The flip the disc suffers is limited by the mass of accreted cooled gas relative to the mass in the disc. In panel (iii), we show the case where only a small amount of cooled gas is accreted relative to the gas mass that was already in the disc, driving a small flip. The outcome of this processes is a misalignment α_{flip} between the gas disc and the DM halo and an angle $\alpha_{G, S}$ between the gas disc and the stellar body.

iv) $t=t_1+\Delta t+\Delta t_{SF}$

v) $t=t_1+\Delta t+\Delta t_{SF}$

- Dark matter
- Hot gas
- Cold gas
- Stellar body
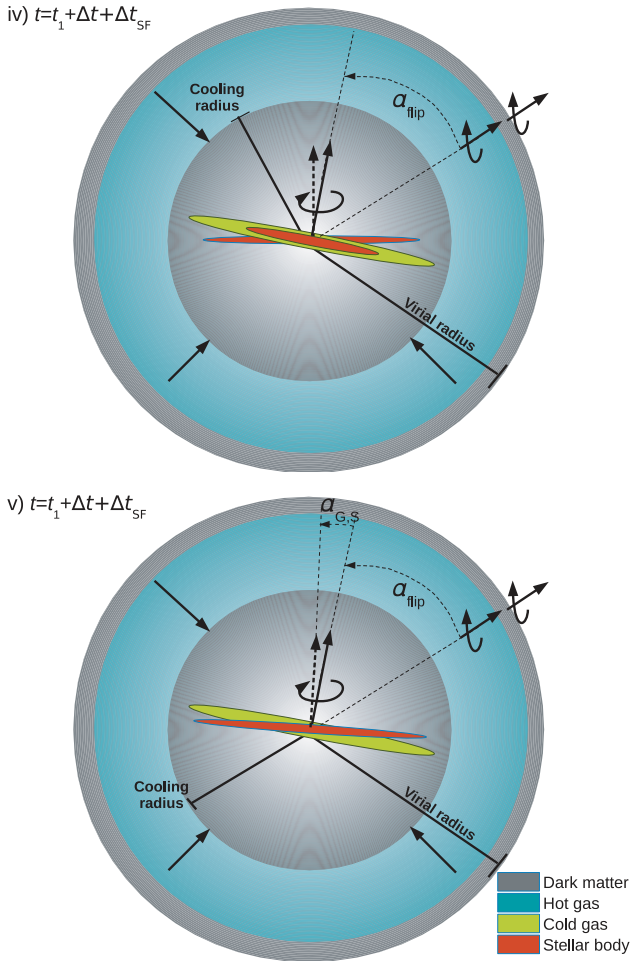
Figure 2. Continuation of Fig. 1. In panel (iv), we show that the cold gas disc has been flipped due to the recent gas accretion. Stars form in this flipped gas disc in a time-scale Δt_{SF}. The angular momentum of the stellar disc is shown by the dashed arrow. In (v), we show the resulting flip in the stellar disc due to the formation of new stars, which had a different angular momentum direction than that of the older stars. In this example, the newly formed stars represent a lower mass than the older stars, which is not enough to flip the stellar disc back into alignment with the gas disc. Therefore, there is a residual angle between the angular momenta of the gas disc and the stars, $\alpha_{G,S}$.

SF episode will affect the direction of the angular momentum of the bulge as a result. This means that when we talk about stellar component we mean bulge plus disc, and assume these are always aligned with each other. This is supported by theoretical work that shows how the components slew to each other to align their angular momenta (Binney & May 1986).

(vi) During disc instabilities, the cold gas is consumed in a starburst and therefore loses its memory of the flips it had accumulated over time, while stars preserve this memory. In a subsequent gas accretion episode, the gas will come with the angular momentum direction of the current hot halo, and may form stars. We calculate the change these newly born stars produce in the angular momentum vector of the stellar body as we explained above (see panel vi in Fig. 2).

(vii) In the case there is a galaxy merger, we take the PDFs corresponding to the galaxy merger case (see Appendix A), and then we apply the same methodology as above to get the new angle

between the angular momenta of the cold gas and stellar body. For the same fractional change in mass, galaxy mergers tend to produce larger flips in the angular momentum direction than results from gas accretion.

Since the growth history is recorded for each ETGs at the output times of the simulation, we perform the above calculations at every timestep, producing a history for the angle between the angular momenta of the different components of ETGs. An important assumption in this model is that consequent flips in the angular momenta of the galaxy components are not correlated. This means that flips can change the angular momenta in random directions, and are not necessarily correlated with the direction at previous times. We test this assumption in Section 6.

Note that in this model we do not take into account any relaxation of the gas disc towards the stellar component due to torques. In the case of the DM component this is implicitly included, as the distributions of flips was obtained by Padilla et al. (2014) using an *N*-body simulation, which includes the gravitational interactions. If the gas is faster in its relaxation than the DM components, then the calculation here would represent upper limits for the angle between the gas and the stellar components of ETGs. An important consideration is that this is done for individual galaxies in their subhaloes. This prevents central galaxies from changing their angular momentum direction due to substructures in the halo. In other words, central galaxies are not affected by changes in the angular momenta of their satellite galaxies (unless they merge).

In observations, the measured position angle of the gas is measured in ionized and molecular gas, which are aligned, suggesting a common origin (Davis et al. 2011). However, in our model we treat the cold gas, which includes atomic and molecular gas, as a single component, and therefore we do not distinguish possible misalignments between H_I and H_2. In observations, H_I is not always aligned with H_2, and indeed a 30 per cent of ETGs show unsettle H_I morphologies (Serra et al. 2012), while this percentage in the case of H_2 is much lower. We simplified the problem by considering the bulk neutral gas and in our model this approximation might not be so critical as the neutral gas that is subject to environmental interactions is the lower density gas which does not contributes so significantly to the total neutral gas mass.

4 THE HISTORY AND MORPHOLOGICAL DEVELOPMENT OF ETGs

Morphology is a transient property of galaxies that is tightly connected to their growth history. This is because it depends on the ability of galaxies to grow galaxy discs after events which lead to spheroid formation, such as disc instabilities or galaxy mergers. Throughout the paper we consider ETGs at $z = 0$ in the Lacey14+GRP model, which we selected to have $L_K > 6 \times 10^9 L_K$, $M_{H_I+H_2} > 10^7$, $M_\odot$ and $M_{bulge}/M_{tot} > 0.5$, where L_K is the *K*-band luminosity, $M_{H_I+H_2}$ is the mass of H_I plus H_2, M_{bulge} is the stellar mass in the bulge and M_{tot} is the total stellar mass of the galaxy. These selection criteria are adopted to mimic the selection criteria of ATLAS^{3D} (see Paper I for details).

In order to help visualize the transient nature of morphology, we show in Fig. 3 the bulge-to-total stellar mass ratio, B/T, of randomly selected ETGs in different present-day stellar mass bins, separating central galaxies (solid lines) from satellites (dashed lines). The first interesting feature is that massive galaxies tend to have had an early-type morphology (i.e. $B/T > 0.5$) for a longer period than lower mass galaxies. This is seen in the example cases of Fig. 3, and also applies
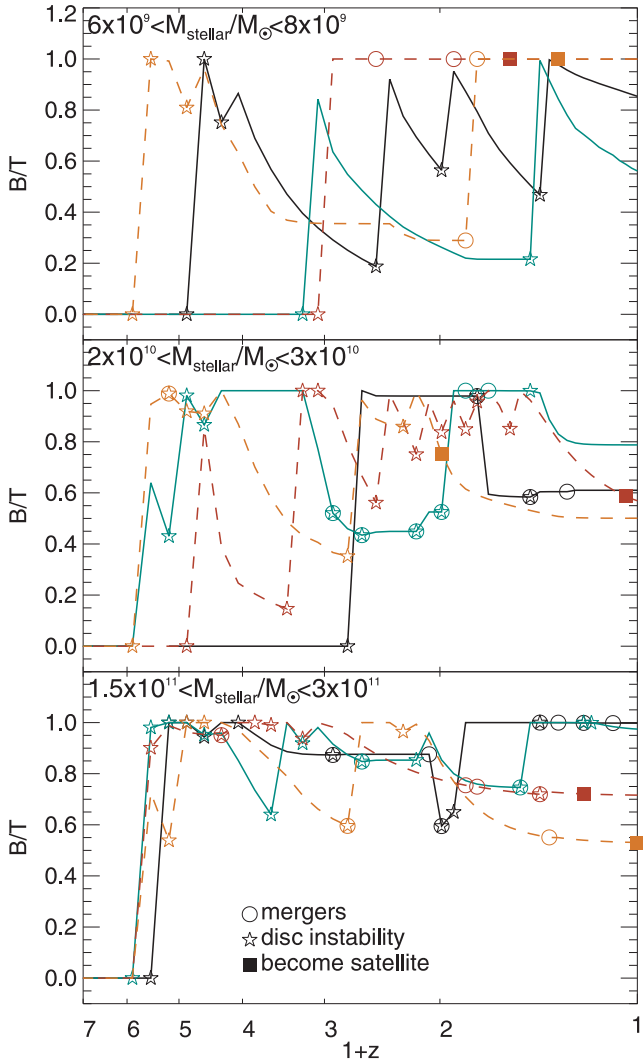
Figure 3. Bulge-to-total stellar mass ratio as a function of redshift for four randomly selected galaxies with present-day stellar masses in three different ranges, as labelled. Solid lines correspond to randomly selected present-day central galaxies, while dashed lines show satellite galaxies. Using symbols we show where each galaxy undergoes a galaxy merger (circles), disc instability (stars) and when it becomes satellite (filled square).

to the general ETG population. The cause of this difference between massive and lower mass ETGs is that low-mass galaxies tend to regrow their disc more efficiently than more massive galaxies. In the case of the most massive galaxies, this is typically due to AGN feedback preventing the formation of a new disc. This was discussed in detail in Paper I. The more efficient regrowth of galaxy discs in the lower mass ETGs is due to the continuous accretion of newly cooled gas. The reason why gas accretion continues even at later times (see, for example, the central galaxy in the top panel of Fig. 3 that has a $B/T = 0.56$ at $z = 0$) is that these ETGs are hosted by lower mass haloes ($M_{halo} \lesssim 5 \times 10^{11}$ M$_\odot$) and have no AGN to heat cooling flows. Central galaxies in the middle and bottom panels of Fig. 3 are hosted by higher mass haloes, $M_{halo} \gtrsim 10^{12}$ M$_\odot$. We also show in Fig. 3, the times when galaxies underwent galaxy mergers and disc instabilities, and in the case of satellite galaxies, we show when they were accreted on to their current halo.

Note that every time a galaxy in the model displays a rapid growth in its B/T ratio, this is due to a galaxy merger or disc instability,

as can be seen in the example galaxies in Fig. 3. Also note that not all galaxy mergers lead to higher B/T, but in some cases there is an associated growth of the disc (see, for example, one of the central galaxies in the bottom panel of Fig. 3 that had a galaxy merger at $z = 1.1$). This can happen during minor mergers with very small satellite-to-central galaxy mass ratios. In the case of model satellite galaxies, there can be disc regrowth once they become satellites in the case of gradual ram-pressure stripping (which is implemented in the Lacey14+GRP model we use here). An example of this is the satellite galaxies in the middle panel of Fig. 3, which continue their disc regrowth, compared to a satellite galaxy in the bottom panel, which stops growing its B/T ratio. The satellite galaxies in the middle panel of Fig. 3 show regrow of their discs as a consequence of the gradual ram-pressure stripping mechanism included in the Lacey14+GRP model, as opposed to the strangulation scenario that results in no further gas cooling. The satellite galaxy of the bottom panel of Fig. 3 that became a satellite at $z \approx 0.3$ does not show any disc regrowth (i.e. its B/T does not significantly change in the time the galaxy has been satellite). The reason for this is that the halo mass of the latter galaxy is higher than those of the satellite galaxies in the middle panel of Fig. 3. This translates into ram-pressure stripping being more efficient in the former case.

Very different stellar mass assembly histories can lead to galaxies having an early-type morphology, as the example galaxies of Fig. 3 show. The specific history of each ETG is expected to have a strong effect on the alignment of their stellar, gas and DM components. In the model of Padilla et al. (2014), every galaxy merger, disc instability and smooth accretion event is considered when following the angular momenta flips. We use the individual gas accretion history of every ETG to estimate their angular momenta alignments in the next section.

## 5 THE ORIGIN OF MISALIGNED GAS DISCS IN ETGS

In this section, we discuss the expected frequency of ETGs that have gas discs misaligned with their stellar component in the Lacey14+GRP model. We compare extensively with the observations of the ATLAS[3D], which are discussed in detail in Davis et al. (2011). We find that the percentage of misaligned gas discs and stellar components in the ETGs of ATLAS[3D] is $\approx 42 \pm 6$ per cent.[7]

5.1 Lower limits on the number of misaligned gas discs in ETGs

In order to show how much misalignment is expected from mergers alone, we post-process the ETGs selected from the Lacey14+GRP model using the Padilla et al. (2014) scheme, but we do not apply any misalignment due to gas accretion from the hot halo. The results of this exercise are shown in Fig. 4. If we only allow mergers to drive misalignments, the model fails to reproduce the observed tail of ETGs that have angles between the angular momenta of the stars and the cold disc, $\alpha_{G, S} > 30$ deg. We find 2 per cent of ETGs with $\alpha_{G, S} > 30$ deg. This percentage increases to 5 per cent in the case we adopt the Lacey & Cole (1993) dynamical friction time-scale. This indicates that other sources of misaligned gas are important if the model is to agree with the observations.

The fractions calculated above represent lower limits as it is assumed that gas accretion on to galaxies from processes other than

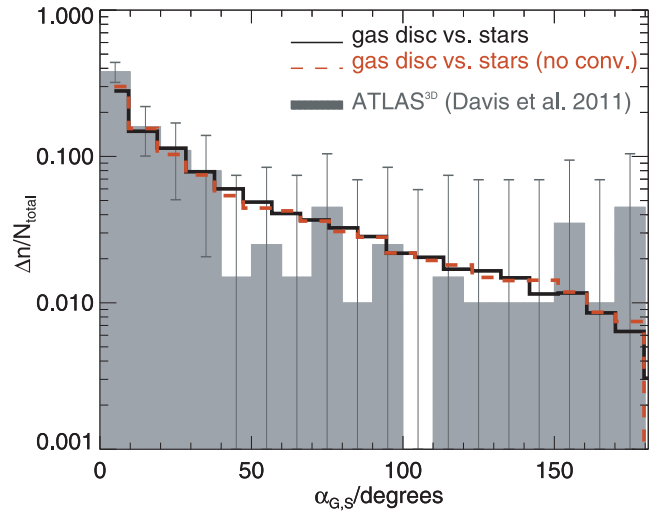[7] The error in this percentage correspond to a Poisson error.
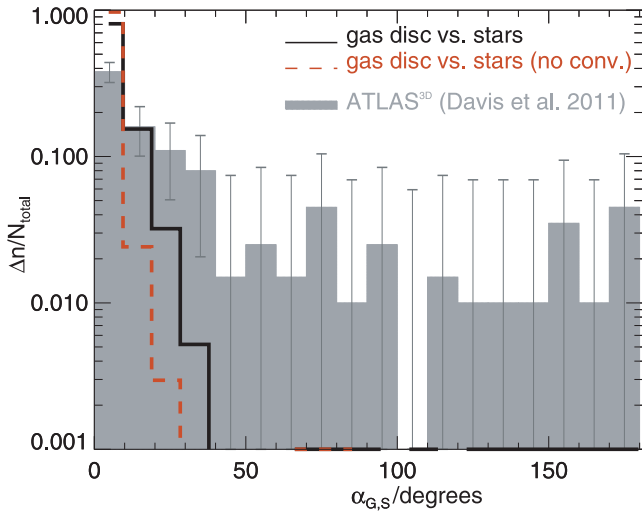
Figure 4. Distribution of angles between the angular momenta of the gas disc and the stellar component, $\alpha_{G,S}$ (dashed line), for ETGs with $L_K > 6 \times 10^9$, $L_\odot$ and $M_{H_I} + M_{H_2} > 10^7$ $M_\odot$ in the Lacey14+GRP model, under the test case that the only source of misaligned gas is galaxy mergers. Observational measurements from ATLAS^{3D} are shown by the shaded histogram. Error bars are Poisson errors. The y-axis is normalized to represent fractions (number of galaxies in the bin divided by the total number in the sample). We convolve the predicted distribution of angles with a normalized Gaussian distribution with its centre at 0 deg and a standard deviation of 15 deg (solid line), which corresponds to the expected scatter in the observations reported by Davis et al. (2011).

galaxy mergers come in perfectly aligned with the stellar body. In Paper I, we show that the vast majority of recent galaxy mergers (i.e. those that took place in the last 1 Gyr) correspond to minor mergers that drive starbursts only in 10 per cent of cases. The remaining 90 per cent correspond to the accretion of small galaxies on to the larger ETGs. Of all ETGs with cold gas masses $M_{H_I+H_2} > 10^7$ $M_\odot$, the percentage that have their current cold gas content supplied mainly by galaxy mergers ranges from 11 to 25 per cent. The main driver of the variation in this percentage is the adopted dynamical friction time-scale. Adopting the Jiang et al. (2008) dynamical friction time-scale, as in Lacey14, leads to earlier minor mergers and consequently a lower merger rate at $z = 0$, leading to the 11 per cent figure referred to above. On the other hand, adopting the Lacey & Cole (1993) dynamical friction time-scale, as in the models of Lagos et al. (2012) and Gonzalez-Perez et al. (2014), leads to a higher rate of minor mergers at $z = 0$, corresponding to the 25 per cent value referred to above. However, these mergers do not necessarily cause a notable change in the angular momentum of the stellar and/or cold gas bodies. In fact the calculation of Padilla et al. (2014) shows that galaxy mergers produce larger angular momentum flips than other forms of accretion but the angle between the angular momentum of the haloes before and after the merger is likely to be small (see Appendix A). This angle also depends on the mass ratio between the two galaxies. This is the reason why a relatively high fraction of ETGs have their current gas content supplied mainly by galaxy mergers, but do not show significant misalignments.

5.2 The distribution of misaligned gas discs in ETGs due to the history of angular momenta flips

We now apply the full scheme introduced by Padilla et al. (2014) to GALFORM galaxies as a more complete calculation than that in

Figure 5. Distribution of angles between the angular momenta of the gas disc and the stellar component, $\alpha_{G,S}$ (dashed line), and after the convolution with a Gaussian of width 15 deg (solid line), for ETGs with $L_K > 6 \times 10^9$, $L_\odot$ and $M_{H_I} + M_{H_2} > 10^7$ $M_\odot$ in the Lacey14+GRP model. Here, we fully apply the Padilla et al. (2014) Monte Carlo method. The y-axis is normalized to represent fractions (number of galaxies in the bin divided by the total number in the sample). Observational measurements are as in Fig. 4.

Section 5.1. We remind the reader that we take the mass growth history of ETGs from the Lacey14+GRP model and post-process it to follow the flips of the angular momenta. The full calculation of Padilla et al. (2014) includes changes in the direction of the angular momenta of galaxy components due to both galaxy mergers and the accretion of cooled gas from the hot halo.

Fig. 5 shows the predicted distribution function of the angle between the cold gas (H$_I$+H$_2$) and the stellar component of ETGs, $\alpha_{G,S}$. We also show these distributions after convolving with a Gaussian distribution with its centre at 0 deg and a standard deviation of 15 deg, which corresponds to the expected scatter in the observations of (Davis et al. 2011). Observations of the ATLAS^{3D} reported by Davis et al. (2011) are shown by the solid histogram with the error bars corresponding to Poission errors. The application of the angular momentum flips model described in Section 3 leads to 46 per cent of ETGs having $\alpha_{G,S} > 30$ deg and a distribution of $\alpha_{G,S}$ that agrees with the observed distribution of ETGs within the error bars (in Section 6, we quantify the agreement between the model predictions and observations using the Kolmogorov–Smirnov test). This is interpreted as misalignment arising not only from recent mergers, as was assumed in Section 5.1, but also from the accretion history of ETGs, which can slew the angular momentum of the stellar component over time with respect to the DM halo and also the gas.

We find that the angle $\alpha_{G,S}$ of each galaxy is strongly affected by recent accretion on to the galaxy compared to the time when the galaxy assembled its stellar mass.[8] We find that if galaxies assembled 80 per cent of their stellar mass before the last episode of cold gas accretion (either from gas cooling from the hot halo or galaxy mergers), they are more likely to show misalignments between the angular momenta of the cold gas and the stellar component. Indeed,

---

[8] We define this as the time the galaxy had assembled 80 per cent of its $z = 0$ stellar mass.

we find that ETGs that have $\alpha_{G,S} > 30$ deg at $z = 0$ assembled 80 per cent of their stellar mass by $z \approx 0.6$, while their last important gas accretion episode took place later at $z \approx 0.3$, on average. On the other hand, in the sample of ETGs with $\alpha_{G,S} < 30$ deg at $z = 0$, we find that 80 per cent of their stellar mass was assembled by $z \approx 0.7$, while their last important gas accretion episode took place at around the same time, on average. This happens because the new gas accretion episodes do not contribute strongly to the stellar mass, and so they hardly change the direction of the angular momentum of stars, while the cold gas can be greatly affected if the change in cold gas mass is important.

This result is shown in the top panel of Fig. 6, where we show the redshift of the last cold gas accretion episode of ETGs (either due to gas cooling from the hot halo or a galaxy merger), z_{LG}, as a function of $\alpha_{G,S}$. This cold gas accretion episode can have any mass, but it is on average quite significant; the median cold mass accreted in this last accretion episode is $3 \times 10^9\,M_\odot$ for ETGs with $M_{stellar} = 10^{10}$ and $7 \times 10^8\,M_\odot$ for ETGs with $M_{stellar} = 10^{11}\,M_\odot$. We also show the median $\alpha_{G,S}$ for bins in z_{LG} and vice versa to show the dominant trends. Recent accretion can lead either to aligned or misaligned cold gas/stellar components, which can be seen from the higher density of galaxies at low z_{LG} regardless of the value of $\alpha_{G,S}$. All ETGs with earlier last cold gas accretion episodes have more aligned stellar and gas components. This is clear from the median $\alpha_{G,S} \approx 10$ deg of galaxies that have $z_{LG} > 3$. Similarly, the median value of $z_{LG} \approx 1$ for galaxies with $\alpha_{G,S} \sim 0$ is higher than for galaxies with higher values of $\alpha_{G,S}$. Note that the median $\alpha_{G,S}$ increases for decreasing z_{LG}.

Another important property that is strongly correlated with the formation time and accretion history of galaxies, and therefore with $\alpha_{G,S}$, is the mass of the subhalo that hosts an ETG. The bottom panel of Fig. 6 shows that misalignment happens in our model only in intermediate ranges of subhalo masses, $7 \times 10^{10}\,M_\odot < M_{subhalo} < 10^{13}\,M_\odot$. The main halo is the largest gravitationally bound structure, which are identify in the N-body simulation using the friends-of-friends algorithm (Davis et al. 1985). Haloes can contain substructures that are self-gravitating, which are call subhaloes and are identify using subfinder algorithms (Knebe et al. 2013, see Jiang et al. 2014 for a recent description on how haloes and subhaloes are identified and followed in the N-body simulations used by GALFORM). The most massive subhalo within haloes generally hosts the central galaxy, while lower mass subhaloes contain satellite galaxies. Not all satellites retain information about their subhalo given that the DM halo can get heavily stripped so that is not considered a substructure within the main halo anymore. In these cases the subhalo mass corresponds to the mass of the subhalo the last time it was identified in the simulation. In the case of ETGs living in massive subhaloes, $M_{subhalo} > 10^{13}\,M_\odot$, most of the gas accretion took place at higher redshifts, where most of the SF happened. This leads to alignment between the angular momenta of the stars and the gas; for $M_{subhalo} > 10^{13}\,M_\odot$, the median $\alpha_{G,S} \approx 8$ deg, while for a halo mass of $M_{subhalo} \approx 3 \times 10^{11}\,M_\odot$ the median $\alpha_{G,S} \approx 50$ deg. Similarly, the median halo mass of low $\alpha_{G,S}$ is higher than for higher values of $\alpha_{G,S}$. Large misalignments, for example $\alpha_{G,S} > 90$ deg, are exclusive of ETGs hosted by haloes $7 \times 10^{10}\,M_\odot < M_{subhalo} < 3 \times 10^{12}\,M_\odot$.

In the case of the lowest mass subhaloes, galaxies have undergone a quieter history, with fewer interactions relative to ETGs hosted by larger mass haloes. This leads the ETG population hosted by low-mass subhaloes to having fewer ETGs with $\alpha_{G,S} > 30$ deg than is the case of ETGs hosted by higher mass subhaloes.
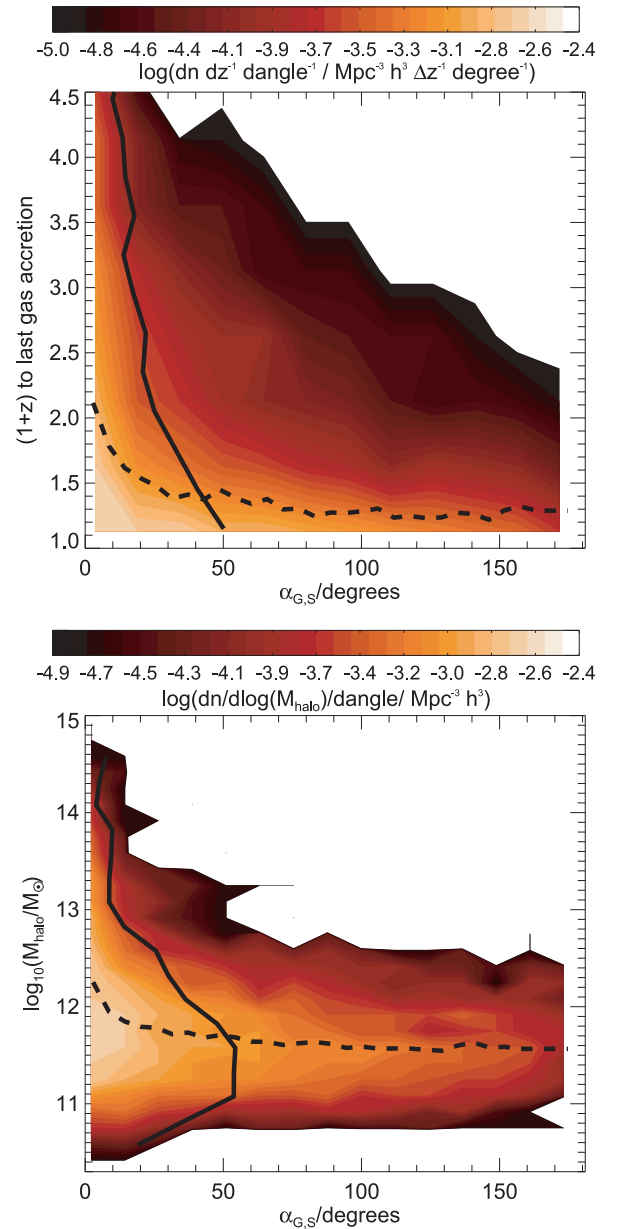
Figure 6. Top panel: the redshift to the last time each ETG had a gas accretion episode (either due to gas cooling from the hot halo or galaxy mergers), z_{LG}, as a function $\alpha_{G,S}$ in the Lacey14+GRP model. Here, we include the same model galaxies as Fig. 5. The coloured contours show number density per unit redshift and angle, with the scale shown by the key (here dz and d angle are the bins in redshift and angle, respectively). The solid line shows the median $\alpha_{G,S}$ for bins in z_{LG}, while the dashed line shows the median z_{LG} for bins in $\alpha_{G,S}$. Bottom panel: as in the top panel but here we show the subhalo mass where the ETG resides. Here, dlog(M_{halo}) and d angle are the bins in halo mass and angle, respectively.

5.2.1 Variance from field to field

An important question that arises from a sample such as ATLAS^{3D}, which is complete up to a distance of 42 Mpc, is what is the effect of the large-scale structure on the statistical analysis we have performed in Section 5.2 (i.e. cosmic variance)? In other words, if we were to observe different volumes of 3×10^5 Mpc^3 (which corresponds to a cube of side $\approx$68 Mpc), how much variance would we
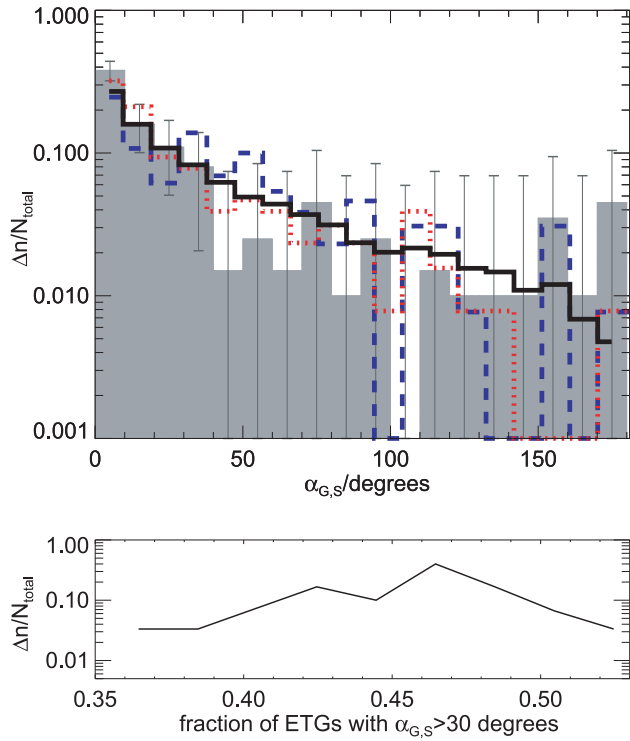
Figure 7. Top panel: distribution of $\alpha_{G,S}$ for ETGs with $L_K > 6 \times 10^9$, $L_\odot$ and $M_{H\,I} + M_{H_2} > 10^7$ $M_\odot$ in the Lacey14+GRP model, and for the realisations of the ATLAS^{3D} volume (3×10^5 Mpc^3) that give the highest (dashed line), median (solid line) and lowest (dot–dashed line) fraction of ETGs with $\alpha_{G,S} > 30$ deg. The observed ATLAS^{3D} distribution is shown by the solid histogram. Bottom panel: distribution of the fraction of ETGs that have $\alpha_{G,S} > 30$ deg in the 30 realizations done of the ATLAS^{3D} volume in the Lacey14+GRP model. The median of the distribution is 46 per cent.

observe in the distribution of $\alpha_{G,S}$? In this section, we investigate the variance of the distribution of $\alpha_{G,S}$.

We make a random selection of 30 subvolumes within the MS-W7 simulation, with each having a volume of 3×10^5 Mpc^3. The resulting distribution of this experiment and the fraction of ETGs with $\alpha_{G,S} > 30$ deg that result are shown in Fig. 7. We find that the percentage of ETGs that have $\alpha_{G,S} > 30$ deg can vary from 35–53 per cent, with a median of 46 per cent. This translates into a variance of ≈ 25 per cent in the volume probed by ATLAS^{3D}. This number agrees very well with the variance as a function of probed volume reported by Driver & Robotham (2010).

We also find that the number of ETGs selected to have $L_K > 6 \times 10^9$ $L_\odot$ and a mass of H$\scriptstyle\rm I$ plus H$_2$ $> 10^7$ $M_\odot$ is on average 300 in each subvolume of 3×10^5 Mpc^3. This number is very close to the number 260 of ETGs in the ATLAS^{3D}. These variations are quite large and we find that the observed sample of ETGs would need to be extended up to 100 Mpc to reduce the variance in the fraction of ETGs with $\alpha_{G,S} > 30$ deg to a few percent.

5.2.2 *Dependence on galaxy properties*

In this section, we focus on the galaxy properties we find are correlated with $\alpha_{G,S}$ and analyse the physical drivers of such correlations. These properties are K-band luminosity and stellar mass, cold gas fraction, satellite/central dichotomy and the SFR. We find no strong dependence of the distribution of $\alpha_{G,S}$ on other galaxy properties,
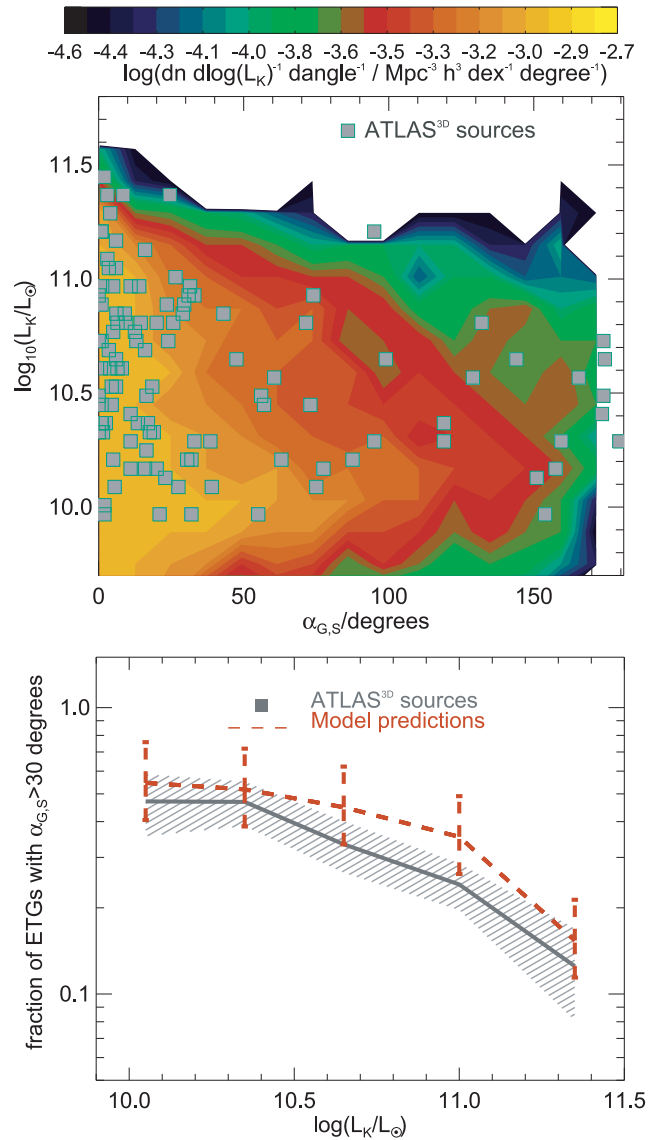
Figure 8. Top panel: K-band luminosity as a function of the angle between the neutral gas and stellar component, $\alpha_{G,S}$, for simulated ETGs from the Lacey14+GRP model and observations from the ATLAS^{3D} survey (Davis et al. 2011). The contours show number density per unit K-band luminosity and angle, as indicated by the colour bar. Here, dlog(L_K) and d angle are the bins in K-band luminosity and angle, respectively. Bottom panel: the fraction of ETGs that have $\alpha_{G,S} > 30$ deg as a function of the K-band luminosity. Observational measurements from the ATLAS^{3D} are shown by the solid line and hatched region, where the latter corresponds to the Poisson error bars. In the model predictions, the error bars correspond to the variations in the fraction due to variance from field to field (which we discuss in Section 5.2.1).

such as bulge-to-total stellar mass ratio or total neutral gas mass (H$\scriptstyle\rm I$ plus H$_2$).

K-*band luminosity and stellar mass.* We find that K-band luminosity (often used as a proxy for stellar mass) is anticorrelated with the angle between the angular momenta of the cold gas and the stellar component, $\alpha_{G,S}$. The top panel of Fig. 8 shows the K-band luminosity as a function of $\alpha_{G,S}$. Overlaid are observations of individual galaxies from the ATLAS^{3D} survey (Davis et al. 2011).
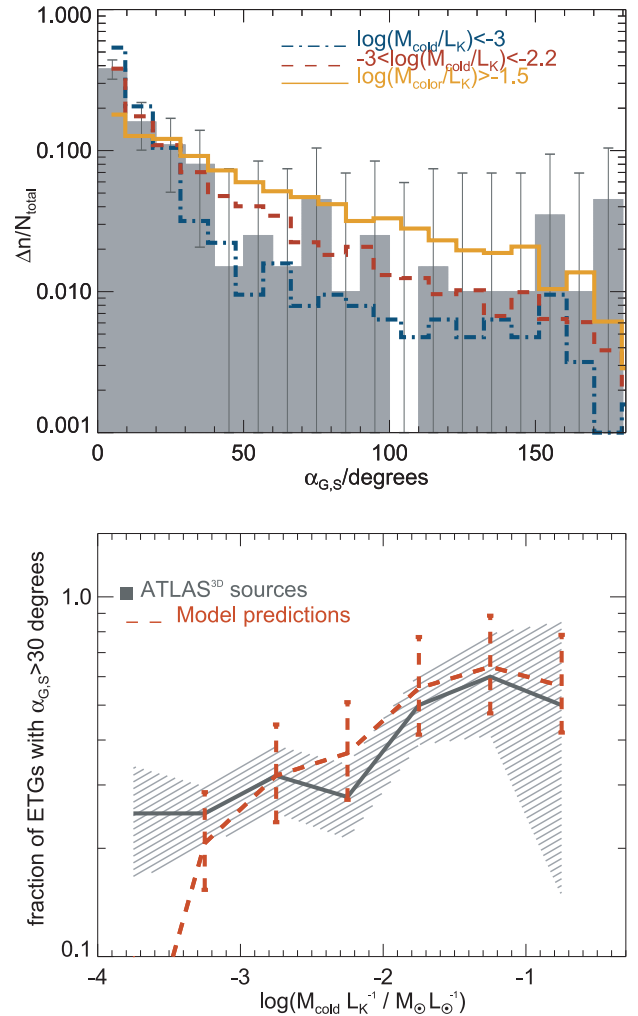
The distribution of $\alpha_{G,S}$ seen in the ATLAS^{3D} observations is very similar to the predictions of the model: there is a higher number density of galaxies at $\alpha_{G,S} < 30$ deg, with the density of galaxies decreasing towards $\alpha_{G,S} > 30$ deg, but with galaxies covering the full range of $\alpha_{G,S}$ at $L_K < 2 \times 10^{11}$ L$_\odot$. At higher K-band luminosities, the model predicts that ETGs show aligned gas and stellar components, with the largest angles being $\alpha_{G,S} \approx 20$ deg, in agreement with the observations. These galaxies reside in the highest mass haloes, with a median subhalo mass of $M_{halo} \approx 9 \times 10^{13}$ M$_\odot$ (shown in Fig. 6), which explains why the model predicts a correlation between K-band luminosity and $\alpha_{G,S}$. For instance, ETGs with 6×10^9 L$_\odot < L_K < 10^{10}$ L$_\odot$, have on average its last cold gas accretion episode at $z \approx 0.3$, while 80 per cent of the stellar mass of these ETGs was in place at $z \approx 0.4$. In contrast, ETGs with $L_K > 3 \times 10^{11}$ L$_\odot$ had the last cold gas accretion episode on average at $z \approx 2.2$, while 80 per cent of the stellar mass of these ETGs was in place only by $z \approx 0.2$.[9] The latter is due to AGN feedback acting on the most massive galaxies from early-on. We have repeated this experiment with stellar mass rather than K-band luminosity and find the same trends.

In order to quantify the agreement with the observations, we calculate the fraction of ETGs in the model and the observations that have $\alpha_{G,S} < 30$ deg in bins of K-band luminosity. The results of this experiment are shown in the bottom panel of Fig. 8. For the observations, we calculate Poisson error bars, which are shown by the hatched region, while for the simulations we calculate an error bar associated with the variance expected from field to field, which we discuss in Section 5.2.1. There is good agreement between the observations and the model. Previous calculations by Dubois et al. (2014) point to stellar mass being strongly correlated with the spin of galaxies and hence is a good indicator of whether the angular momentum of the galaxy is aligned with the halo. However, Dubois et al. do not analyse the alignments between the different galaxy components.

Gas Fraction. We find that the cold gas fraction, expressed as the ratio between the H I+H$_2$ mass and the K-band luminosity, is correlated with the level of misalignment between the angular momenta of the cold gas disc and the stellar component such that galaxies with low cold gas fractions tend to be more aligned than galaxies that are gas-rich. This is shown in the top panel of Fig. 9. Galaxies with high cold gas fractions typically have had recent cold gas accretion, which have changed the cold gas content considerably, while their stellar mass has not changed significantly over the same time-scale. The effect of this is that the angular momentum of the stellar body is only mildly modified by the newly formed stars, while the angular momentum of the cold gas changes considerably. The gas fraction here is correlated with the recent gas accretion history. We find that this relation holds even when we look at galaxies in a narrow range of stellar masses, pointing to this correlation being independent of stellar mass.

Serra et al. (2014) show that there is a trend of galaxies with low H I fractions to show alignments between the stellar and H I components, while misalignments are more likely in ETGs with higher H I gas fractions. This trend agrees qualitatively with our predictions. We quantify this trend by calculating the fraction of ETGs that have $\alpha_{G,S} > 30$ deg as a function of cold gas fraction,

---

[9] Note that the time-scale we discuss here for the stellar mass build-up is an assembly age rather than a stellar age. This is because the stellar ages of these galaxies are much higher than the assembly age (see, for example, Baugh, Cole & Frenk 1996; Kauffmann 1996).

Figure 9. Top panel: distribution of $\alpha_{G,S}$ in ETGs with $L_K > 6 \times 10^9$ L$_\odot$ in the Lacey14+GRP model and in different bins of cold gas fraction, $M_{H\,I+H_2}/L_K$[M$_\odot$/L$_\odot$]. Observational measurements from the ATLAS^{3D} are shown by the shaded histogram. The y-axis is normalized to represent fractions. Bottom panel: as in the bottom panel of Fig. 8, but here we show the fraction of ETGs that have $\alpha_{G,S} > 30$ deg as a function of the cold gas fraction.

(H I+H$_2$)/L_K, for ETGs in both simulations and observations. In the case of non-detections of H I and/or CO for ATLAS^{3D} galaxies, we take the value of the upper limit on the H I and/or H$_2$ mass. The results are shown in the bottom panel of Fig. 9, where the error bars are as in the bottom panel of Fig. 8. We find that the correlation predicted by the model between $\alpha_{G,S}$ and cold gas fraction is also observed in the ATLAS^{3D}, which is reassuring. This is evidence that our model contains some of the mechanisms that drive the misalignments observed in ATLAS^{3D}.

Satellites versus centrals. Fig. 10 shows the histogram of the angle between the angular momenta of the cold gas and stellar components in ETGs, separating central and satellite galaxies. There is a trend for satellite galaxies to show misalignments more often than centrals. Satellite galaxies in the model are quenched by ram-pressure stripping of the hot gas and SNe driven winds. The former start operating when the galaxy becomes a satellite. Overall, this results in satellite galaxies having 80 per cent of their stellar mass in place earlier than central galaxies, which exhibit more recent SF.
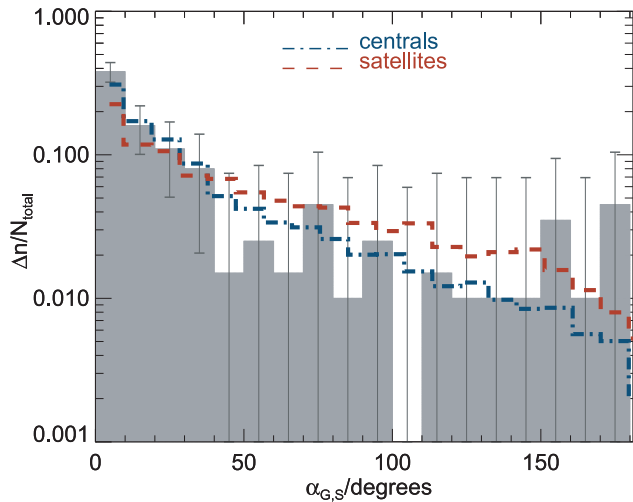
Figure 10. As in the top panel of Fig. 9 but for central and satellite galaxies.

For satellites, accretion of cold gas on to the galaxy can continue for as long as the satellite retains part of its hot gas halo. However, a lot of this cold gas is too low density to transform into H_2, resulting in low SFRs that do not alter the stellar mass of the galaxy. In the case of central galaxies, both SF and accretion of cold gas continue for longer which leads to higher levels of alignment between the two components. Unfortunately, we cannot test this prediction with the current available data, but with larger data sets than ATLAS[3D] we would be able to cross-match with group catalogues and test this idea.

Note that the trend of satellite/centrals is not driven by stellar mass. We can see this by fixing the stellar mass and then looking at satellite and central galaxies. As an example, for the stellar mass bin $10^{10}\,M_\odot < M_{stellar} < 3 \times 10^{10}\,M_\odot$, the fraction of satellite ETGs with $\alpha_{G,S} > 30$ deg is 62 per cent, while for centrals this fraction is 45 per cent. However, there is a strong connection between the frequency of misalignments in centrals and satellites and the range of subhalo masses hosting these two galaxy populations. The median subhalo mass of satellite ETGs in the model is $M_{subhalo} \approx 3 \times 10^{11}\,M_\odot$, where the peak of the frequency of misalignments takes place (see bottom panel of Fig. 6). On the other hand, the median subhalo mass of central ETGs in the model is $M_{subhalo} \approx 10^{12}\,M_\odot$.

Star formation rate. Fig. 11 shows the distribution of $\alpha_{G,S}$ in three different bins of SFR. We find that in the model, ETGs with low SFRs are associated with a preference for lower values of $\alpha_{G,S}$ compared to those with higher SFRs. This is because higher SFRs in ETGs are associated with important recent cold gas accretion. Note that a similar trend is found between $\alpha_{G,S}$ and the specific SFR (SSFR – the ratio between the SFR and the stellar mass); i.e. galaxies with lower SSFR show lower values of $\alpha_{G,S}$. At a fixed stellar mass we find that the correlation between $\alpha_{G,S}$ and SFR becomes stronger. This is because stellar mass is positively correlated with SFR but anticorrelated with $\alpha_{G,S}$. Thus, when plotting all stellar masses the positive correlation between SFR and $\alpha_{G,S}$ becomes weaker. Note however, that the driver of the correlation of $\alpha_{G,S}$ with SFR and cold gas fraction is the same and therefore they are not independent.

We test the existence of a correlation between $\alpha_{G,S}$ and SFR using ATLAS[3D] and the measured SFRs presented by Davis et al. (2014). Davis et al. measured SFRs in ETGs using a combination of
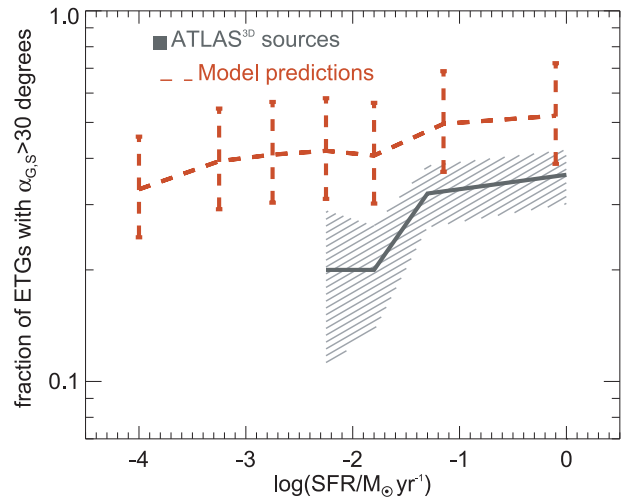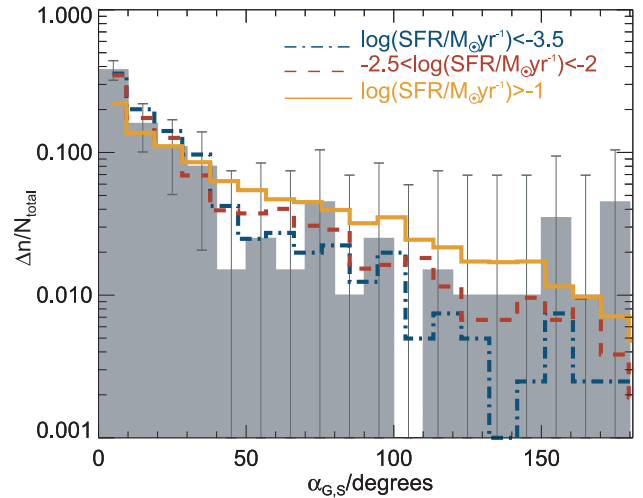

Figure 11. As in Fig. 9 but for bins of SFR. In ATLAS[3D], there are SFRs available from *WISE*, and combined with *GALEX* for galaxies that have detection in the far-UV, for only 56 sources (Davis et al. 2014). This is why the statistics worsen when plotted as a function of the SFR compared to the trends shown in the bottom panel of Fig. 9.

ultraviolet information from *GALEX* and infrared photometry from *WISE*, when far-UV photometry was available, or only *WISE* data when not far-UV was available. This was possible for a subsample of 56 ETGs. This worsens the statistics, but nevertheless we perform the calculation of the fraction of ETGs with $\alpha_{G,S} > 30$ deg as a function of SFR to reveal possible trends. This is shown in the bottom panel of Fig. 11. The model predictions are also shown. The observations suggest a trend that goes in the same direction as the predictions of our model. It would be possible to confirm such a trend if SFRs were available for all ETGs in the ATLAS[3D], as is the case of the cold gas fraction.

6 LIMITATIONS OF THE MODEL AND DISCUSSION

An important assumption of the model of Padilla et al. (2014) is that flips in the angular momenta of the galaxy components are uncorrelated over time. This means that an angular momentum flip at a given time, for instance, of the gas disc, has a direction uncorrelated
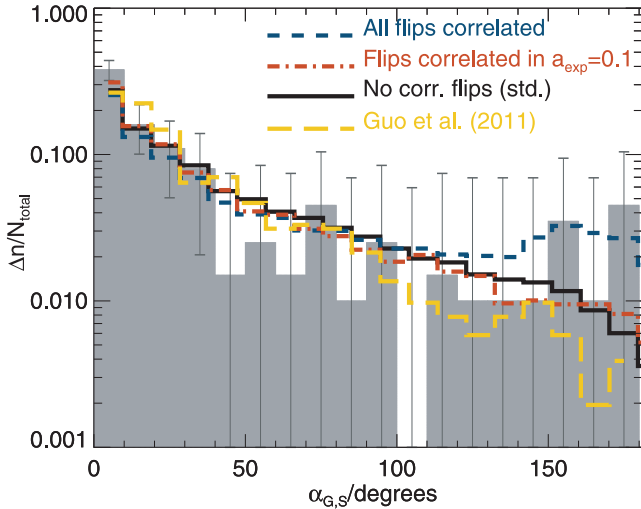
Figure 12. Distribution of angles between the angular momenta of the cold gas disc (H I+H$_2$) and the stellar body, $\alpha_{G,S}$, for ETGs with $L_K > 6 \times 10^9$, L$_\odot$ and $M_{H_1} + M_{H_2} > 10^7$ M$_\odot$ in the Lacey14+GRP model, when we consider no correlated angular momentum flips over time (standard model; solid line), when all flips are correlated in direction over time (dashed line), and when flips are correlated only during finite time intervals (i.e. during an interval of expansion factor $a_{exp} = 0.1$; dot–dashed line). We also show the predicted distribution of $\alpha_{G,S}$ from the semi-analytic model of Guo et al. (2011).

Table 1. The two-sided KS probability, p_{KS}, calculated using galaxies from ATLAS^{3D} and the Lacey14+GRP model under the scenario of no correlated flips over time, all flips correlated over time and flips correlated only over an interval in expansion factor of $a_{exp} = 0.1$. We also show the value of p_{KS} for the publicly available model of Guo et al. (2011).

Model	p_{KS}
No flips correlated (Lacey14+GRP)	0.16
All flips correlated (Lacey14+GRP)	0.002
Flips correlated over $a_{exp} = 0.1$ (Lacey14+GRP)	0.04
Guo et al. (2011)	0.0001

to the direction of previous flips. This is not necessarily the case in reality, as matter can come in from preferred directions, for example from filaments. These filaments bring large specific angular momentum compared to that of the halo, and hence are capable of changing the direction of the galaxy angular momentum towards the preferred direction of filaments (Pichon et al. 2011; Sales et al. 2012; Danovich et al. 2012, 2014; Aumer et al. 2013). This means that subsequent accretion episodes can come from the same (or similar) directions, which translates into angular momentum flips being correlated in direction over time.

The ability of these cold flows to reach the halo centre where galaxies live is under debate. For example, Nelson et al. (2013) suggest that cold streams do not self-shield as efficiently as previously thought, as there is important heating as cold streams travel through the DM halo towards the centre. They show that the maximum fraction of gas accreted on to galaxies that did not get shock heated to a temperature close to the virial temperature of the halo is ≈0.3 for a present-day halo mass of 5×10^{10} M$_\odot$ h^{-1}. This fraction decreases with increasing halo mass. Thus, it is still unclear to what extent angular momentum flips can be correlated in direction over time.

Here, we test the idea of all flips in angular momentum being correlated in direction over time, and compare this assumption with our standard model, which assumes uncorrelated flips. Fig. 12 shows the histogram of $\alpha_{G,S}$ for our standard model and for the model when all flips are correlated in direction over time. The latter model produces a flatter distribution of $\alpha_{G,S}$, particularly at $\alpha_{G,S} > 100$ deg. The fraction of galaxies with $\alpha_{G,S} > 30$ deg rises from 46 per cent in our standard model to 52 per cent. In order to quantify which model produces results closer to the observed one we calculate the two-sided Kolmogorov–Smirnov (KS) probability, p_{KS} (calculated using the ATLAS^{3D} results). The values of p_{KS} are shown in Table 1 for the standard model (i.e. uncorrelated flips) and for the realization that assumes correlated flips over time.

From the values in Table 1, one can conclude that observations prefer flips in angular momenta that are not fully correlated over time, i.e. the direction of flips in angular momentum at any time cannot know about all previous flips. Another possibility is that if correlated flips exit, the correlation spans time-scales that are shorter than the age of galaxies. In order to test this idea, we perform an experiment where flips are correlated in direction during a finite period of time. We choose to quantify this by the interval in expansion factor where flips are correlated, a_{exp}. We show the result of this experiment for $a_{exp} = 0.1$ in Fig. 12 and the results of the KS test in Table 1. This model predicts a fraction of galaxies with $\alpha_{G,S} > 30$ deg of 48 per cent and from the results of Table 1 one can conclude that the model using uncorrelated flips is still in better agreement with the observations.

We also show for reference in Fig. 12 the predictions from a different semi-analytic model, that of Guo et al. (2011). In this model they follow the 3D angular momenta of the gas and stars in galaxies along similar lines to those presented in Section 3. In Guo et al., stars and gas are treated as independent bodies and they do not react to the gravity of each other as in GALFORM. The predicted distribution of $\alpha_{G,S}$ also agrees well with the observations. We calculate a KS probability and the result is presented in Table 1. The Guo et al. model gives slightly worse agreement with the observations of the ATLAS^{3D} than our standard model. The fact that the model of Guo et al. following a similar scheme as we presented here also predicts a distribution of $\alpha_{G,S}$ in reasonable agreement with the observations points to the robustness of such prediction even when physical processes in galaxies are treated differently in different models. Unfortunately, semi-analytic models are limited by their simplified geometries, and it is not possible to include collimated flows feeding galaxies. Further studies with fully consistent cosmological hydrodynamic simulations are needed for this task. Cosmological simulations such as EAGLE (Schaye et al. 2015) and Illustris (Vogelsberger et al. 2014) are ideal for this.

Another interesting result from hydrodynamical simulations is that the rotation of stars can enhance cooling from the hot halo (Negri et al. 2014). This may be of particular interest for the fast rotators found in ATLAS^{3D} (Cappellari et al. 2011). However, in the simulation setup of Negri et al. (2014), mass-loss from stars feeds the halo of galaxies from which cooling takes place. This means that the system is designed to have components which are preferentially aligned. We show in Paper I that the fraction of ETGs have their ISM content dominated by this gas source is very small (≈2 per cent), and therefore this may be a second-order effect in our calculations. A more complete study, for example using cosmological

hydrodynamical simulations can constrain the importance of this mechanism in driving accretion on to galaxies.

6.1 Expectations for LTGs

The distribution of $\alpha_{\mathrm{G,S}}$ for LTGs (bulge-to-total stellar mass ratio <0.5) will soon be probed by integral field surveys, such as SAMI, MANGA and CALIFA, and therefore it is important to show predictions for this population. The top panel of Fig. 13 shows the distribution of $\alpha_{\mathrm{G,S}}$ for LTGs and ETGs that have $M_{\mathrm{stellar}} > 10^8 \, \mathrm{M}_\odot$ and $M_{\mathrm{H\,I}} + M_{\mathrm{H_2}} > 10^7 \, \mathrm{M}_\odot$. The distribution for central galaxies only is also shown. LTGs are expected to show slightly higher levels of misalignments than ETGs. However, the exact fraction of galaxies with $\alpha_{\mathrm{G,S}} > 30$ deg is a strong function of stellar mass. Note that the anticorrelation discussed in Section 5.2.2 between the fraction of ETGs with $\alpha_{\mathrm{G,S}} > 30$ deg and *K*-band luminosity (or stellar mass) reverses at $M_{\mathrm{stellar}} \approx 10^{10} \, \mathrm{M}_\odot$ for ETGs and at $M_{\mathrm{stellar}} \approx 3 \times 10^{10} \, \mathrm{M}_\odot$ for LTGs, with lower mass galaxies having a lower frequency of $\alpha_{\mathrm{G,S}} > 30$ deg. If this turnover exists, the large

Figure 13. Top panel: distribution of $\alpha_{\mathrm{G,S}}$ for ETGs ($B/T > 0.5$) and LTGs ($B/T < 0.5$) with $M_{\mathrm{stellar}} > 10^8 \, \mathrm{M}_\odot$ and $M_{\mathrm{H\,I}} + M_{\mathrm{H_2}} > 10^7 \, \mathrm{M}_\odot$ in the Lacey14+GRP model when we fully apply the Padilla et al. (2014) Monte Carlo method. We show all galaxies of each morphological type, as well as centrals only, as labelled. Bottom panel: the fraction of galaxies with $\alpha_{\mathrm{G,S}} > 30$ deg as a function of stellar mass for the same model galaxy populations shown in the top panel.

galaxy catalogue probed by SAMI will be able to see it. The driver of this turnover is due to an important fraction of galaxies below the turnover mass living in haloes with masses $M_{\mathrm{subhalo}} < 5 \times 10^{11} \, \mathrm{M}_\odot$. These galaxies have had a quieter history, with fewer interactions relative to galaxies living in more massive haloes. The galaxies in low-mass halo show more alignments than galaxies in intermediate halo masses (see Fig. 6).

In the case of LTGs, torques would be stronger since the gas has a clear disc to which to relax. Since we do not explicitly account for torques our calculation would be upper limits.
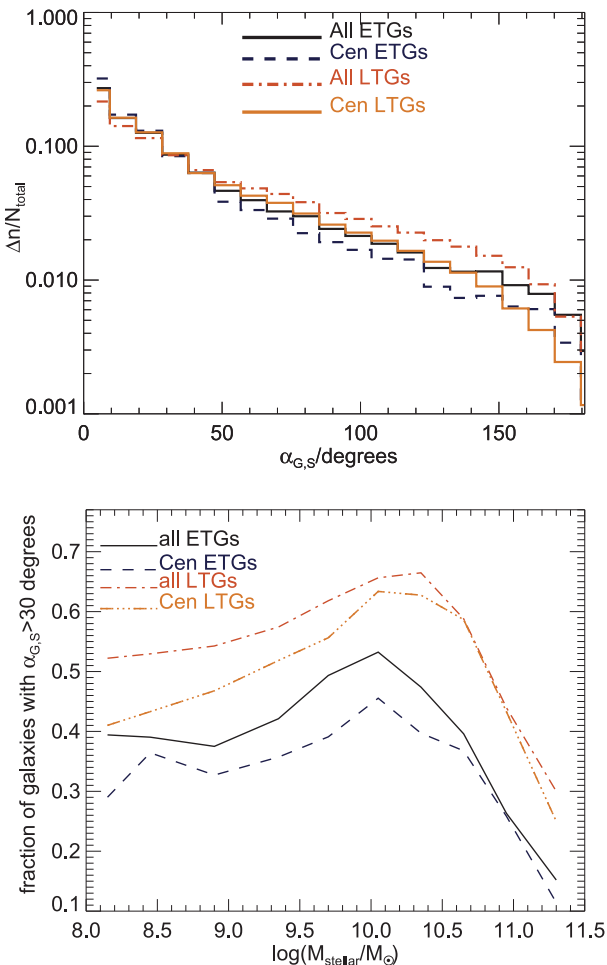
7 CONCLUSIONS

We have explored the origin of misalignments between the stars and gas in ETGs in the local Universe using the Lacey14 variant of the GALFORM model. The reference observational data set is the ATLAS$^{3\mathrm{D}}$ survey, which displays a fraction of 42 ± 6 per cent of ETGs exhibiting angles between the angular momenta of the gas and stars of $\alpha_{\mathrm{G,S}} > 30$ deg. This paper is the second of the series. We show in Paper I that the Lacey14 model reproduces the H I and H$_2$ gas fractions and gas mass distribution functions of ETGs very well. The key to the latter is the incorporation of gradual ram-pressure stripping (see Paper I for details).

We first explore the simplest assumption, which is that the only source of misaligned cold gas (H I plus H$_2$) with respect to the stellar body in ETGs is galaxy mergers. This has traditionally been the observational interpretation of of misaligned cold gas discs (Davis et al. 2011; Serra et al. 2012). However, we find that there are not enough galaxy mergers at $z \approx 0$ in the model, regardless of the dynamical friction time-scale adopted. We find that by adopting the Jiang et al. (2008) dynamical time-scale, which is the default option in Lacey14, only 11 per cent of ETGs in the model have had a minor merger in the last 1 Gyr that involved important gas accretion, leading to only 2 per cent of ETGs having $\alpha_{\mathrm{G,S}} > 30$ deg. This percentage rises to ≈ 5 per cent if we use the Lacey & Cole (1993) dynamical friction time-scale, which favours more recent minor mergers.

We then explore a more general approach, which is to follow the history of gas accretion and stellar growth due to SF *in situ* and due to galaxy mergers, and apply the Monte Carlo simulation of Padilla et al. (2014) to follow the angular momenta flips that are produced by this growth. This simulation analyses the change in mass and the source of that change (i.e. smooth accretion or mergers) and returns PDFs of the angle between the direction of the angular momentum of the component that is changing in mass before and after the accretion. That angle can change in any direction and we accumulate the change over time. We do this for all the components of ETGs we are interested in: hot halo, cold gas disc (H I plus H$_2$) and stellar component. We apply this procedure for all ETGs in the semi-analytic model that have been selected to mimic the ETG selection in the ATLAS$^{3\mathrm{D}}$ survey (based on their *K*-band luminosity and H I+H$_2$ mass). Our main findings are as follows.

(i) By applying the Padilla et al. Monte Carlo simulation to the ETGs predicted by the Lacey14 model, we find that 46 per cent of modelled ETGs have $\alpha_{\mathrm{G,S}} > 30$ deg. This angle varies in the range 35–53 per cent when we select subvolumes of the simulation of the size of the volume probed by the ATLAS$^{3\mathrm{D}}$ (which observed all ETGs with $L_{\mathrm{K}} > 6 \times 10^9 \, \mathrm{L}_\odot$ out to 42 Mpc). The level of misalignment found agrees with the observations, within the error bars. Note that our model has not been tuned to reproduce this observable and therefore this is a true prediction of the model.

(ii) We find that misalignments ($\alpha_{G,S} > 30$ deg) are found in ETGs living in intermediate-mass haloes ($7 \times 10^{10}\,M_\odot < M_{halo}/h < 10^{13}\,M_\odot$), while ETGs hosted by larger or lower mass haloes tend to have $\alpha_{G,S} < 30$ deg. This agrees with the observational results that ETGs living very close to each other (e.g. galaxy clusters or massive galaxy groups) show stellar and gas components that are aligned (Davis et al. 2011).

(iii) We find that the relation between $\alpha_{G,S}$ and the halo mass leads to correlations between $\alpha_{G,S}$, stellar mass, cold gas fraction and SFR. Galaxies in the model with high stellar masses, low SFRs and low cold gas fractions show lower values of $\alpha_{G,S}$. The observational findings from ATLAS[3D] shows that galaxies with $L_K \gtrsim 3 \times 10^{11}\,L_\odot$ show $\alpha_{G,S} < 30$ deg, which agrees very well with our predictions. These show that massive galaxies, $L_K > 3 \times 10^{11}\,L_\odot$, are very unlikely to show misalignments. We also test the prediction that there is a dependence of $\alpha_{G,S}$ on cold gas fraction and SFR using the observations of the ATLAS[3D] and we find that these correlations are also in the observations, and they had not been found before.

(iv) The above trends are understood within the simple phenomenological finding that galaxies that have important gas accretion after most of the stellar mass of the galaxy is in place, are more likely to exhibit cold gas discs misaligned with respect to the stars. This accreted gas can come from either galaxy mergers or smooth cold gas accretion and it is not necessarily aligned with the existing stellar body. Galaxies in the model living in galaxy groups and clusters, which are also the most massive ETGs, lack important recent gas accretion episodes, and therefore their cold gas and stellar mass are aligned.

(v) We show expectations for LTGs and ETGs over a wide range of stellar masses ($M_{stellar} > 10^8\,M_\odot$) and predict the existence of a turnover mass ($M_{to} \approx 10^{10}\,M_\odot$), at which misalignments are most likely The existence of this turnover mass will soon be probed by integral field galaxy surveys.

The Monte Carlo approach applied to GALFORM galaxies offers new, interesting ideas for the origin of what has been observed in ETGs in the local Universe, which has proven elusive in simulations of individual galaxies (Serra et al. 2014). The next step will be to integrate this angular momentum scheme directly into GALFORM to model intrinsic alignments between galaxies. Large improvements can also come from recent hydrodynamical simulations (Vogelsberger et al. 2014; Schaye et al. 2015), which for the first time can tackle the problem of the angular momenta of the different galaxy components from hydrodynamical simulations in a statistical fashion.

ACKNOWLEDGEMENTS

REFERENCES

Alatalo K. et al., 2013, MNRAS, 432, 1796
Aumer M., White S. D. M., Naab T., Scannapieco C., 2013, MNRAS, 434, 3142
Baugh C. M., Cole S., Frenk C. S., 1996, MNRAS, 283, 1361
Baugh C. M., Lacey C. G., Frenk C. S., Granato G. L., Silva L., Bressan A., Benson A. J., Cole S., 2005, MNRAS, 356, 1191
Benson A. J., Bower R., 2010, MNRAS, 405, 1573
Benson A. J., Frenk C. S., Lacey C. G., Baugh C. M., Cole S., 2002, MNRAS, 333, 177
Bett P. E., Frenk C. S., 2012, MNRAS, 420, 3324
Bett P., Eke V., Frenk C. S., Jenkins A., Okamoto T., 2010, MNRAS, 404, 1137
Binney J., May A., 1986, MNRAS, 218, 743
Blitz L., Rosolowsky E., 2006, ApJ, 650, 933
Boselli A., Cortese L., Boquien M., Boissier S., Catinella B., Gavazzi G., Lagos C., Saintonge A., 2014, A&A, 564, 67
Bournaud F. et al., 2011, ApJ, 730, 4
Bournaud F. et al., 2014, ApJ, 780, 57
Bower R. G., Benson A. J., Malbon R., Helly J. C., Frenk C. S., Baugh C. M., Cole S., Lacey C. G., 2006, MNRAS, 370, 645
Boylan-Kolchin M., Springel V., White S. D. M., Jenkins A., Lemson G., 2009, MNRAS, 398, 1150
Bryan S. E., Kay S. T., Duffy A. R., Schaye J., Dalla Vecchia C., Booth C. M., 2013, MNRAS, 429, 3316
Cappellari M. et al., 2011, MNRAS, 416, 1680
Cavaliere A., Fusco-Femiano R., 1976, A&A, 49, 137
Ceverino D., Dekel A., Bournaud F., 2010, MNRAS, 404, 2151
Cole S., Lacey C. G., Baugh C. M., Frenk C. S., 2000, MNRAS, 319, 168
Cortese L., Catinella B., Boissier S., Boselli A., Heinis S., 2011, MNRAS, 415, 1797
Creasey P., Theuns T., Bower R. G., 2013, MNRAS, 429, 1922
Croom S. M. et al., 2012, MNRAS, 421, 872
Danovich M., Dekel A., Hahn O., Teyssier R., 2012, MNRAS, 422, 1732
Danovich M., Dekel A., Hahn O., Ceverino D., Primack J., 2014, preprint (arXiv:1407.7129)
Davis M., Efstathiou G., Frenk C. S., White S. D. M., 1985, ApJ, 292, 371
Davis T. A. et al., 2011, MNRAS, 414, 968
Davis T. A. et al., 2013, MNRAS, 429, 534
Davis T. A. et al., 2014, MNRAS, 444, 3427
Dekel A., Sari R., Ceverino D., 2009, ApJ, 703, 785
Driver S. P., Robotham A. S. G., 2010, MNRAS, 407, 2131
Dubois Y. et al., 2014, MNRAS, 444, 1453
Efstathiou G., Lake G., Negroponte J., 1982, MNRAS, 199, 1069
Emsellem E. et al., 2004, MNRAS, 352, 721
Fanidakis N. et al., 2012, MNRAS, 419, 2797
Font A. S. et al., 2008, MNRAS, 389, 1619
Gallagher J. S., Faber S. M., Balick B., 1975, ApJ, 202, 7
Gonzalez-Perez V., Lacey C. G., Baugh C. M., Lagos C. D. P., Helly J., Campbell D. J. R., Mitchell P. D., 2014, MNRAS, 439, 264
Guo Q. et al., 2011, MNRAS, 413, 101
Husemann B. et al., 2013, A&A, 549, A87
Jiang C. Y., Jing Y. P., Faltenbacher A., Lin W. P., Li C., 2008, ApJ, 675, 1095
Jiang L., Helly J. C., Cole S., Frenk C. S., 2014, MNRAS, 440, 2115
Jiménez N., Cora S. A., Bassino L. P., Tecce T. E., Smith Castelli A. V., 2011, MNRAS, 417, 785
Johansson P. H., Naab T., Ostriker J. P., 2012, ApJ, 754, 115
Kauffmann G., 1996, MNRAS, 281, 487
Kennicutt R. C., Jr, 1983, ApJ, 272, 54
Knebe A. et al., 2013, MNRAS, 435, 1618
Komatsu E. et al., 2011, ApJS, 192, 18
Lacey C., Cole S., 1993, MNRAS, 262, 627

Lagos C. D. P., Cora S. A., Padilla N. D., 2008, MNRAS, 388, 587

Lagos C. D. P., Lacey C. G., Baugh C. M., Bower R. G., Benson A. J., 2011a, MNRAS, 416, 1566

Lagos C. D. P., Baugh C. M., Lacey C. G., Benson A. J., Kim H.-S., Power C., 2011b, MNRAS, 418, 1649

Lagos C. D. P., Bayet E., Baugh C. M., Lacey C. G., Bell T. A., Fanidakis N., Geach J. E., 2012, MNRAS, 426, 2142

Lagos C. D. P., Lacey C. G., Baugh C. M., 2013, MNRAS, 436, 1787

Lagos C. D. P., Baugh C. M., Zwaan M. A., Lacey C. G., Gonzalez-Perez V., Power C., Swinbank A. M., van Kampen E., 2014a, MNRAS, 440, 920

Lagos C. D. P., Davis T. A., Lacey C. G., Zwaan M. A., Baugh C. M., Gonzalez-Perez V., Padilla N. D., 2014b, MNRAS, 443, 1002 (Paper I)

McCarthy I. G., Frenk C. S., Font A. S., Lacey C. G., Bower R. G., Mitchell N. L., Balogh M. L., Theuns T., 2008, MNRAS, 383, 593

Marigo P., 2001, A&A, 370, 194

Mitchell P. D., Lacey C. G., Cole S., Baugh C. M., 2014, MNRAS, 444, 2637

Mo H. J., Mao S., White S. D. M., 1998, MNRAS, 295, 319

Morganti R. et al., 2006, MNRAS, 371, 157

Murray N., Quataert E., Thompson T. A., 2005, ApJ, 618, 569

Naab T. et al., 2014, MNRAS, 444, 3357

Negri A., Posacki S., Pellegrini S., Ciotti L., 2014, MNRAS, 445, 1351

Nelson D., Vogelsberger M., Genel S., Sijacki D., Kereš D., Springel V., Hernquist L., 2013, MNRAS, 429, 3353

Obreschkow D., Glazebrook K., 2014, ApJ, 784, 26

Okamoto T., Gao L., Theuns T., 2008, MNRAS, 390, 920

Oosterloo T., Fraternali F., Sancisi R., 2007, AJ, 134, 1019

Padilla N. D., Salazar-Albornoz S., Contreras S., Cora S. A., Ruiz A. N., 2014, MNRAS, 443, 2801

Pichon C., Pogosyan D., Kimm T., Slyz A., Devriendt J., Dubois Y., 2011, MNRAS, 418, 2493

Portinari L., Chiosi C., Bressan A., 1998, A&A, 334, 505

Ruiz A. N. et al., 2013, preprint (arXiv:1310.7034)

Sales L. V., Navarro J. F., Theuns T., Schaye J., White S. D. M., Frenk C. S., Crain R. A., Dalla Vecchia C., 2012, MNRAS, 423, 1544

Schaye J. et al., 2015, MNRAS, 446, 521

Serra P. et al., 2012, MNRAS, 422, 1835

Serra P. et al., 2014, MNRAS, 444, 3388

Sharma S., Steinmetz M., Bland-Hawthorn J., 2012, ApJ, 750, 107

Springel V. et al., 2005, Nature, 435, 629

Sutherland R. S., Dopita M. A., 1993, ApJS, 88, 253

Tenneti A., Mandelbaum R., Di Matteo T., Feng Y., Khandai N., 2014, MNRAS, 441, 470

Vogelsberger M. et al., 2014, Nature, 509, 177

Wardle M., Knapp G. R., 1986, AJ, 91, 23

Welch G. A., Sage L. J., Young L. M., 2010, ApJ, 725, 100

Wiklind T., Henkel C., 1989, A&A, 225, 1

Young L. M. et al., 2011, MNRAS, 414, 940

Young L. M. et al., 2014, MNRAS, 444, 3408

## APPENDIX A: PDFS OF ANGULAR MOMENTUM FLIPS AND SLEWS

In Fig. A1, we show the PDFs for the angle between the angular momentum of DM haloes in the Millennium-II before and after
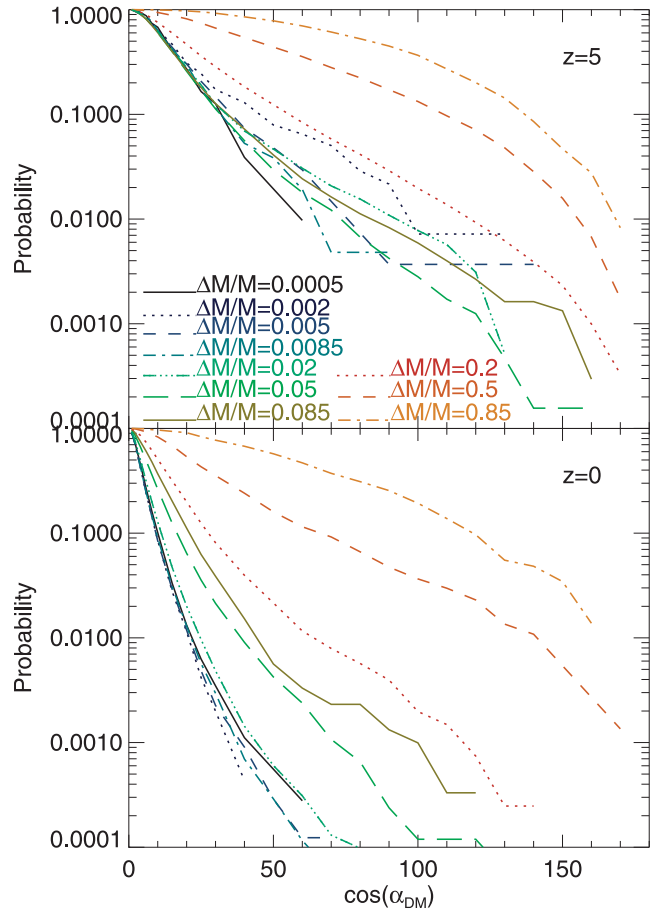
Figure A1. PDFs of the angle between the angular momentum of DM haloes before and after accretion of matter (excluding halo mergers). Each line corresponds to a different fractional change as labelled in the top panel. The top panel shows PDFs at $z = 5$, while the bottom panel shows the PDFs at $z = 0$. These PDFs were calculated in the Millennium-II simulation by Padilla et al. (2014).

they have accreted mass as calculated by Padilla et al. (2014). Each line corresponds to a fractional change in mass and we show these PDFs for two different redshifts. Fig. A2 shows the same PDFs but for flips in the angular momentum due to mergers with other DM haloes.
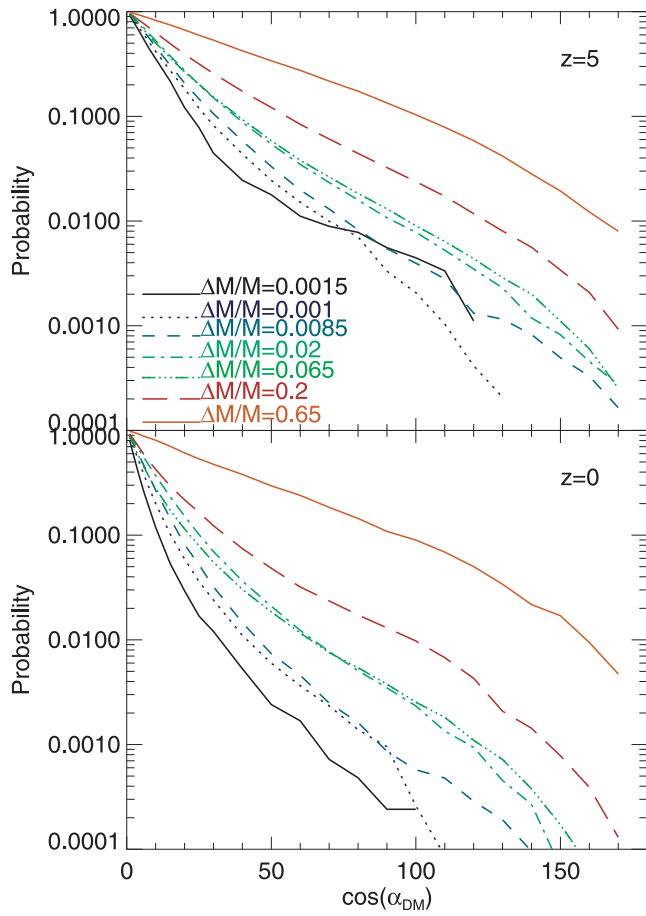
Figure A2. As in Fig. A1 but here we show the flips in the angular momentum of DM haloes only due to mergers with other DM haloes. The fractional change in mass due to mergers are as labelled in the top panel.

This paper has been typeset from a TEX/LATEX file prepared by the author.